MUSA SANI MUSA SIMULATION AND EVALUATION OF A COST-EFFECTIVE HIGH-PERFORMANCE BRAIN PET SCANNER NEU 2018

SIMULATION AND EVALUATION OF A COST-EFFECTIVE HIGH-PERFORMANCE BRAIN PET SCANNER

A THESIS SUBMITTED TO THE GRADUATE SCHOOL OF APPLIED SCIENCES OF NEAR EAST UNIVERSITY

By
MUSA SANI MUSA

In Partial Fulfillment of the Requirements for the Degree of Master of Science in Biomedical Engineering

NICOSIA, 2018

SIMULATION AND EVALUATION OF A COST-EFFECTIVE HIGH-PERFORMANCE BRAIN PET SCANNER

A THESIS SUBMITTED TO THE GRADUATE SCHOOL OF APPLIED SCIENCES OF NEAR EAST UNIVERSITY

By
MUSA SANI MUSA

In Partial Fulfillment of the Requirements for the Degree of Master of Science in Biomedical Engineering

NICOSIA, 2018

Musa Sani MUSA: SIMULATION AND EVALUATION OF A COST-EFFECTIVE HIGH-PERFORMANCE BRAIN PET SCANNER

Approval of Director of Graduate School of Applied Sciences

Prof. Dr. Nadire ÇAVUŞ

We certify this thesis is satisfactory for the award of the degree of Master of Science in Biomedical Engineering

Examining Committee in Charge:

Prof. Dr. Rahib H. Abiyev	Committee Chairman, Department of Computer Engineering, NEU
Prof. Dr. Kerem Cankoçak	Department of Physics Engineering, ITU
Assist. Prof. Dr. Dilber Uzun Özşahin	Supervisor, Department of Biomedical Engineering, NEU
Assist. Prof. Dr. İlker Özşahin	Co-Supervisor, Department of Biomedical Engineering, NEU
Assist. Prof. Dr. Sertan Kaymak	Department of Electrical and Electronics Engineering, NEU

I hereby declare that all information in this document has been obtained and presented in accordance with academic rules and ethical conduct. I also declare that, as required by these rules and conduct, I have fully cited and referenced all material and results that are not original to this work.

Name, Last name:

Signature:

Date:

ACKNOWLEGMENTS

First and foremost, I would want to express my earnest appreciation to my humble supervisor Assist. Prof. Dr. Dilber Uzun Özşahin and my Co-Supervisor Assist. Prof. Dr. İlker Özşahin for their ceaseless support & guidance, and for providing me with all the required skills and research tools to complete my thesis within the stipulated time. In addition, my gratitude goes to Near East University, Department of Biomedical engineering and Assoc. Prof. Dr. Terin Adali for helping me through my academic journey.

To my Late parents Alh. Sani Musa Dan-hassan and Haj. Hauwa Saeed, my Late GrandMa Haj. Aisha Alhassan, words alone can't express how grateful I am for the support you gave me during your life time. I miss you so much and love you to the moon and back. May your souls continue to rest in perfect peace.

For bye, my most profound thanks and ardent love goes to my brothers Alh. Bello & Nasir Sani Musa, my sisters Haj. Aisha, Amina, Hauwa, Fatima and Sa'adatu Samudan, my step Mum Haj. Habiba Sani Idris and my entire family for their consistent support and help amid my thesis writing.

To my Uncle Alh. Auwal Saeed, my Aunties Haj. Hafsat and Haj. Hadiza, my beloved 2nd mother Haj. Halima Sabiu Bako, I thank you for all you have done to me in this life. May Allah reward you abundantly

Lastly, I would also like to thank Alh. Sani Ibrahim, Alh. Sani Salisu, Haj. Sa'adatu Musa, Mr. Mubarak yakubu for their support, including my friends who took their time to share with me their knowledge.

To my parents...

ABSTRACT

Positron Emission Tomography (PET) perform exceptionally in functional imaging, primarily for cancer detection. Most commercialized PET system designs are dedicated to the whole body (WB) studies with a few dedicated to organs like the brain, heart and breast. Organ dedicated scanners have reduced field of view (FOV) which makes them perform excellently in the course of diagnosis than WB scanners. Brain studies require systems with high sensitivity and spatial resolution due to the pathologies associated with the brain. On the one hand, semiconductor-based PET detectors have an excellent intrinsic spatial resolution but are not cost-effective. On the other hand, scintillator-based PET detectors can provide high system sensitivity and are cost effective, but they lack the spatial resolution required to detect very small brain lesions. Therefore, the spatial resolution of such detectors needs to be improved. Focusing improved spatial resolution of scintillator crystals, a brain PET scanner ("MB-PET") based on $1\times1\times10$ mm^3 pixelated lutetium yttrium oxyorthosilicate (LYSO) detector was simulated using Geant4 application for emission tomography (GATE) simulation, and its performance was evaluated following the National electrical manufacturers association (NEMA) NU 4-2008 standards. The complete scanner has 35.0 cm detector ring diameter, 24.5 cm axial FOV and trans-axial FOV of 31.0 cm. Spatial resolution varied across CFOV from approximately 1.0 to 1.28 mm Full width at half maximum (FWHM) in the trans-axial direction and from 1.03 to 2.05 mm (FWHM) in the axial direction. The scanner can provide 4.8% system sensitivity and a scatter fraction of 48%.

Keywords: Brain PET; GATE; MLEM; LYSO scintillator; CdTe

ÖZET

Pozitron Emisyon Tomografisi (PET), kanser tespiti için fonksiyonel görüntülemede çok önemli rol oynamaktadır. Genel olarak hastanelerde kullanılan PET sistemi tasarımı çoğunlukla tüm vücut (WB) çalışmalarına ayrılmıştır. Diğer taraftan küçük organ merkezli tarayıcılarının daha küçük görüş alanına (FOV) sahip olmasından dolayı, WB tarayıcılarından daha iyi performans sergilediği bilinmektedir. Beyin çalışmaları, beyin ile ilişkili patolojilere bağlı olarak yüksek duyarlılık ve uzaysal çözünürlüğe sahip sistemlere ihtiyaç duymaktadır. Yarıiletken tabanlı PET dedektörler, mükemmel uzaysal çözünürlüğe sahiptir, ancak maliyet açısından uygun değildir. Diğer yandan, sintilatör tabanlı PET dedektörler, yüksek sistem hassasiyeti sağlayabilir ve maliyet açısından etkili olmasına karşın, çok küçük beyin lezyonlarını saptamak için gereken uzaysal çözünürlükten yoksundurlar. Bu nedenle, bu dedektörlerin uzaysal çözünürlüğü geliştirilmelidir. Bu çalışmada sintilatör kristallerinin geliştirilmiş uzaysal çözünürlüğüne odaklanarak, 1x1x10 mm3 pikselli lutetiyum itriyum oksiortosilikat (LYSO) kristallerine dayanan beyin PET tarayıcısı ("MB-PET"), GATE simülasyonu kullanılarak simüle edildi ve performansı, NEMA NU 4-2008 standartlarına göre değerlendirildi. Tarayıcının geometrisi, 35.0 cm çapında hasta portu, 24.5 cm eksenel FOV ve 31.0 cm trans-eksenel FOV'ye sahiptir. Uzaysal çözünürlük, eksenel doğrultuda yaklaşık 1.0 ile 1.28 mm (FWHM) ve eksenel yönde 1.03 ile 2.05 mm arasında değişiyor. Tarayıcı, % 4.8 sistem hassasiyeti ve % 48 saçılma fraksiyonu sağlayabilir.

Anahtar Kelimeler: Beyin PET; GATE; MLEM; LYSO Sintilatör; CdTe

TABLE OF CONTENTS

LIST OF TABLES

LIST OF FIGURES

LIST OF ABBREVIATIONS

1D:	One Dimensional
2D:	Two Dimensional
3D:	Three Dimensional
APD:	Avalanche Photo Diodes
BGO:	Bismuth Germanate
Br:	Bromine
C:	Carbon
CdTe:	Cadmium Telluride
CFOV:	Centre Field of View
CNR:	Contrast-Noise-Ratio
CT:	Computed Tomography
CZT:	Cadmium Zinc Telluride
DC:	Direct Current
DOI:	Depth of Interaction
F:	Fluorine
FBP:	Filtered Back Projection
FOV:	Field of View
FT:	Fourier Transform
FWHM:	Full Width at Half Maximum
FWTM:	Full Width at Tenth Maximum
GATE:	Geant4 Application for Emission Tomography
Ge:	Germanium
GSO:	Gadolinium Oxy-Silicate
I:	Iodine
keV:	Kiloelectron Volt
LIOB:	Laser Induced Optical Barrier
LM-OSEM:	List Mode-Ordered Subset Expectation Maximization
LOR:	Line of Response
LSO:	Lutetium Oxyorthosilicate

LuAP:	Lutetium Aluminum Perovskite
LYSO:	Lutetium Yttrium Oxyorthosilicate
MC-PMT:	Multi Channel-Photo Multiplier Tube
MLEM:	Maximum Likelihood Expectation Maximization
MRI:	Magnetic Resonance Imaging
N:	Nitrogen
NaI:	Sodium Iodide
NEMA:	National Electrical Manufacturers Association
O:	Oxygen
OE:	Origin Ensemble
OSEM:	Ordered Subset Expectation Maximization
PET:	Positron Emission Tomography
PMT:	Photo Multiplier Tube
PSF:	Point Spread Function
PS-PMT:	Position Sensitive-Photo Multiplier Tube
RAMLA:	Raw Action Maximum Likelihood Algorithm
RC:	Recovery Co-efficient
Si:	Silicon
SiPMs:	Silicon Photo Multipliers
SNR:	Signal-Noise- Ratio
SPECT:	Single Photon Emission Computed Tomography
SR:	Spatial Resolution
SSRB:	Single Slice Rebinning
TOF:	Time of Flight
WB:	Whole Body

CHAPTER 1
INTRODUCTION

Positron Emission Tomography (PET) is a diagnostic imaging procedure which utilizes pair of "back-to-back" photons originating from positron-electron annihilation for diagnostic purposes (Sweet, 1951). The use of PET has rapidly increased in the field of oncology, cardiology, and neuropsychiatry. It is used on daily basis as a routine diagnostic procedure in brain metabolism, cardiac function, and cancer detection worldwide. Research works aimed at developing high sensitivity and spatial resolution brain scanners are on-going, these researches are being motivated by the increasing interest in functional images to aid early detection of brain tumors and other diseases (Vandenberghe, 2016). Most commercialized PET system designs are dedicated to the whole body (WB) studies with a few dedicated to organs such as brain, heart, and breast (Watanabe et al., 2002). Organ dedicated scanners have reduced field of view (FOV) to the organ of interest which makes them perform excellently at lower cost and also yield excellent results in the course of diagnosis than the WB scanners (Uzun et al., 2014).

The key requirements for high-speed and high resolution PET imaging are detectors with fast decay time, high quantum detection efficiency, high light output, good timing resolution and high counting rate capability. Lutetium oxyorthosilicate (LSO) and Lutetium yttrium oxyorthosilicate (LYSO) both cerium doped are used recently because they have some of these requirements and also perform better than the other scintillator crystals like bismuth germinate (BGO) (Junwei et al., 2009). Therefore, LYSO was used in the present study.

Semiconductor-based PET detectors such as cadmium zinc telluride (CZT) and cadmium telluride (CdTe) have received much attention due to their high energy resolution (Sabet et al., 2016). These detectors, however, have some disadvantages as the segmentation size becomes smaller. Issues include increase in the number of readout electronic channels and its associated complexities which lead to unfavorable cost issues. Scintillator-based detectors, on the other hand, are typically more flexible with lower system cost because the number of electronic channels is smaller than those of the semiconductor. However, they

have problems related to large light spread arising from unstructured scintillators, and the light spread increases with thickness of the scintillator leading to poor spatial resolution. Therefore, the scintillation light has to be controlled in order to provide high spatial resolution (Sabet et al., 2016).

Laser-induced optical barrier (LIOB) is a profitable fabrication method for scintillator crystals which serves as a substitute to mechanical pixelation (Sabet et al., 2012). This method was employed in the present study because of its high efficiency at producing crystals with high intrinsic spatial resolution.

In the present study, a Brain PET scanner employing highly pixelated LYSO scintillator detector was simulated with GATE and the detector performance was evaluated according NEMA NU 4-2008. The performance test includes sensitivity, scatter fraction, spatial resolution, uniformity, and image quality.

1.1 Thesis Problems

- Brain and other nervous system tumors are among the leading cause of cancer-related deaths in males and females ("Brain tumor statistics," 2017).
- Mechanical pixelation of crystals into sub-millimeter size is practically impossible, quite tedious, time consuming, expensive and leads to material lost (Sabet et al., 2012).
- Brain scanners based on scintillator crystals lack the required spatial resolution to detect smaller-sized tumors.
- Brain scanners based on solid state detectors are very expensive.

1.2 Aims of the Study

- To simulate a cost-effective brain PET scanner
- To simulate a high spatial resolution brain PET scanner employing laser processed scintillator crystal
- To simulate a high sensitivity brain PET scanner
- To test the scanner's performance following NEMA guidelines

1.3 Significance of the Study

- The findings of the study will lead to a reduction in mortality rates and improve chances of survival (Jemal, Siegel, Xu & Ward, 2010).
- The findings of this study will demonstrate the ability of a cost-effective scintillator-based brain scanner to achieve high spatial resolution.
- The findings of the study will demonstrate the ability of scintillator-based PET scanners to achieve good sensitivity to detect most of the 511keV photons used in PET scans.
- The findings of the study will serve as reference for future researchers conducting a similar research.

1.4 Limitations of the Study

- The geometry of the simulated scanner is entirely approximate, series of structural changes might be done when developing the true scanner.
- In the simulation, all the 468,480 voxels work perfectly, but in real life, some might be faulty or not function well.
- The output of one detector connected to a chip is difficult to simulate, but a model of the detector behavior can be created and tested.

1.5 Overview of the Thesis

Chapter 1 introduces the thesis and explains the problems, aims, significance and limitations of the study, while chapter 2 explains the literature review and fundamental physics. In chapter 3, the overview of PET imaging technique and PET in Nuclear medicine is presented. Chapter 4 describes the system specifications, simulation and performance evaluation. Chapter 5 explains the result and lastly, Chapter 6 concludes the study and also includes recommendations for future studies.

CHAPTER 2
LITERATURE REVIEW AND THEORETICAL PHYSICS

Mikhaylova et al., (2014) conducted a study which was aimed at evaluating the design of an uncommon Brain PET scanner. The system uses $1\times1\times 2$ mm^3 pixelated cadmium telluride detectors (CdTe), and it has a diameter of 42 cm on the inside, 54 cm on the outside and an axial length of 25.4 cm. The simulated scanner was evaluated following NEMA guidelines. Image reconstruction was done using filtered back projection (FBP) and single slice rebinning technique (SSRT). Evaluation results showed that the sensitivity of the scanner is 14cps/kBq with 3.95% scatter fraction and 21cps/kBq with 0.73% scatter fraction with NEMA NU 2-2001 and NU 4-2008 respectively. Image resolution was 1mm FWHM in all directions.

Watanabe et al., (2002) developed a high-resolution brain PET scanner and they evaluated its physical performance. The PET system is based on $2.8 \times 6.55 \times 30$ mm^3 pixelated BGO, and has a diameter of 508 mm on the outside, 330 mm inside diameter and 163 mm axial length. The geometry used is enough to accommodate the human head. FBP was used to reconstruct the images. Evaluation results showed that 2.9 mm FWHM central FOV spatial resolution was obtained in axial and trans-axial directions. 6.4 kc/s/kBq/ml system sensitivity was achieved in two-dimensional (2-D) mode.

Morimoto et al., (2011) developed a 3D brain PET scanner and evaluated its physical performances which include spatial resolution and sensitivity. The PET scanner which happens to be the first to employ semiconductor detectors was dedicated to both head and neck region. The scanner uses $1.0 \times 4.0 \times 7.5$ mm^3 pixelated CdTe and has a diameter of 35.0 cm on the outside, 31.0 cm inside diameter and 24.6 cm axial length. Images were reconstructed using 2D iterative reconstruction algorithm such as 2D OSEM and FBP, and also 3D iterative reconstruction such as 3D OSEM and Raw-Action maximum likelihood algorithm. Evaluation results according to NEMA 1994 showed that the PET scanner can achieve a sensitivity of 25.9cps/Bq/cm^3 and a spatial resolution of 2.3mm FWHM.

Wienhard et al., (2002) developed a prototype of high resolution brain tomograph and evaluated its performance which include spatial resolution, scatter and sensitivity using phantom studies and measurements with a point source. The PET scanner is a 3D tomograph that employs a $2.1 \times 2.1 \times 7.5$ mm^3 pixelated LSO crystals and has an outer diameter of 35.0 cm, inside diameter of 31.2 cm, and an axial length of 25.2 cm. Images were reconstructed using 3D OSEM algorithm. Evaluation results showed a sensitivity of 4.3% and a spatial resolution of less than 2.4 mm FWHM at the CFOV, and less than 2.8 mm FWHM at 10 cm off center.

Yamaha et al., (2008) evaluated a brain PET scanner prototype. They were able to perform a human brain imaging using the so-called jPET-D4. The system dimensions are 390 mm outside diameter, 300 mm inside diameter and 260 mm axial length. The PET scanner employs Gadolinium oxyorthosilicate (GSO) crystal with $2.9 \times 2.9 \times 7.5$ mm^3 pixelation. Images were reconstructed using histogram based 3D OSEM algorithm and MLEM algorithms. Evaluation results showed that the system has a spatial resolution of less than 3 mm FWHM and 11% sensitivity with energy window of 400-600 keV. Images obtained from phantom and human brain showed that the jPET-D4 has excellent imaging performance.

Karp et al., (2014) developed a high sensitivity and high resolution brain PET scanner called G-PET. The system which is based on $4 \times 4 \times 10$ mm^3 pixelated anger logic GSO detector, has a diameter of 42.0 cm on the outside, 30.0 cm inside diameter and an axial length of 25.6 cm. The scanner is operated in 3D mode due to the absence of interplane septa and was evaluated following NEMA guidelines. Image reconstruction was done with 3D RAMLA and 3D reprojection algorithm. Evaluation results showed that the system can provide 4.79cps/kBq absolute sensitivity using a line source. The achieved transverse image resolution was 4.0 mm and axial resolution of 5.0 mm FWHM. High quality images were also obtained from Hoffman brain phantom and ^{18}F-FDG patient scans.

Li et al., (2006) Developed a transformable ultra-high resolution PET camera which has 54 cm outside diameter and 21 cm axial length for brain/breast studies. This camera is based on $2.7 \times 2.7 \times 18$ mm^3 pixelated BGO detector. Hoffman brain images of good quality were obtained from this camera which were reconstructed with SSRB and 2D FBP. Evaluation result showed that the camera can achieve a sensitivity of 9.2% and trans-axial image resolution of 2.7 mm at CFOV and 4.0 mm at 10 cm from the CFOV of the camera.

Jong et al., (2007) developed a PET scanner called ECAT HRRT for brain and small animal examinations and they evaluated its physical performance. The PET system uses double layer LSO/LYSO and is designed in such a way to perform excellently. NEMA protocols were used as a guideline to estimate the performance of the device. Evaluation results showed that a point source trans-axial spatial resolution was approximately 2.3 to 3.2 mm (FWHM) and axial resolutions was 2.5 to 3.4 mm. The total system sensitivity varies from 2.5 to 3.3% with 45% scatter fraction. This evaluation results showed that the developed system has a promising advantage in research studies.

2.1 Laser Induced Optical Barrier

Laser-induced optical barrier (LIOB) is a cost-effective method used to incorporate optical structures into crystals, and a light guide to control the spread of light. This allows for high resolution and depth of interaction measurement.

It is an alternative method to the conventional (mechanical) method of fabricating crystals which involves focusing a laser beam into the bulk of the scintillator crystal. This makes the crystal structure as well as refractive index changes. Pulse energy, density, wavelength and crystal structure contributes to the size of the damage created on the crystal. Optical barriers serve as reflecting surface that scatters the scintillator photons, they can be constructed in any pattern at numerous depths all over the crystal volume. The simplest pattern is straight walls resembling pixels, which can be used for different materials including hygroscopic scintillators and has the ability to control depth-dependent light spread for depth of DOI measurement. It has a high yield process that leads to fabricate cost-effective scintillator arrays with high intrinsic resolution. Figure 2.1 shows the concept of the LIOB technique.

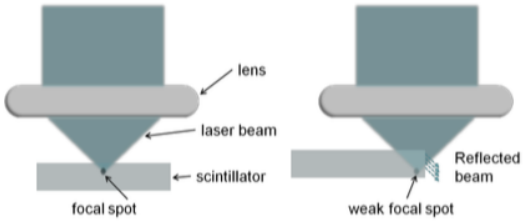

(a) (b)

Figure 2.1: Schematics of the concept of LIOB technique (Sabet et al., 2016)

The process involves focusing a high-intensity laser beam into the bulk of crystal via a lens, this introduces intense heat within the crystal. Scintillators are poor heat conductors, therefore the heat stays within the crystal and causes a regional damage. The size of the area affected by the laser beam can be controlled through optimization of the duration and energy of the laser pulse combined with the delivery optics. Moreover, microstructures with distinct refractive index (RI) with respect to the neighboring medium can be created by optimizing the energy and duration of the laser beam. These microstructures are referred to as optical barriers.

With the optical barriers within the crystal, scintillation light can then be reflected and refracted. The RI of the crystal with respect to the surrounding medium and the angle of incidence of the light photon control the amount of light reflected by a single optical barrier. Having successfully creating the barriers within the crystal, scintillation light can then be effectively redirected and its spread can be controlled leading to improvement in the detector intrinsic spatial resolution.

Furthermore, optical barriers are used to create a reflecting wall that resembles the reflecting material placed between pixels in the conventional mechanical procedure.

NOTE: Apart from creation of pixel-like shapes, the LIOB technique can also be used to create almost any pattern within the crystal. Figure 2.2 shows a picture of scintillator crystal fabricated using the LIOB technique. Optical walls were created using a 140 double pass of laser beam, which was scanned through the scintillator. A second laser scanning followed a little space, that can be of any value (Sabet et al., 2016).

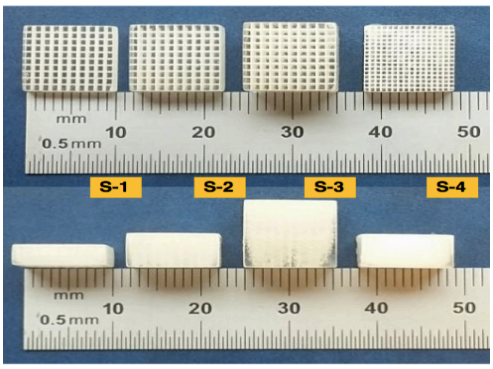

Figure 2.2: Fabricated scintillator arrays using the LIOB technique (Sabet et al., 2016)

2.2 Physics Fundamentals

2.2.1 Discovery of the positron

In the year 1928, Paul Dirac a British scientist wrote down an equation which combines quantum theory and special relativity, while trying to explain the character of an electron that moves at a relativistic speed. Dirac equation appeared to have a problem because two possible solutions could come out of the equation. Paul later interpreted his equation to mean that every existing particle has a corresponding anti-particle with the same mass but opposite charge. In 1931, Dirac forecasted an anti-electron existence having equal mass but of opposite charge with the electron, which he noted that when the two particles interact, they will mutually annihilate. The discovery of Dirac was confirmed in 1933 by Occhialini and Blacket. Another scientist named Anderson proved the existence of this anti-particle and was awarded a Nobel prize in physics in 1936 for discovering the positron. PET imaging got its origin in 1951 when two scientists from Massachusetts General Hospital William Sweet and Gordon Brownell suggested the use of the radiation from Positron-electron annihilation to increase sensitivity and resolution of diagnostic imaging thereby enhancing the quality of brain images. In 1953, these scientists produce the description of the first device for positron-imaging to store 3D brain data ("Discovering the positron", 2017).

2.2.2 Positron production in isotope decays

Positrons were first produced naturally by converting high cosmic-energy radiation into electron-positron pair as observed by Carl Anderson in 1932. Another form of positron production is the famous beta-decay whereby an excess proton is transformed into a neutron, with a positron and electron neutrino emitted as as well (Krane, 1987).

$$P \rightarrow n + \beta^{+} + \nu_e \qquad (2.1)$$

Beta-decay usually takes place in unstable nuclides that have a low atomic number and excess protons. Nowadays, radionuclides that emit positron are often produced in particle accelerators at some major laboratories. A new nucleus (daughter) results from radioactive decay of such unstable nuclides (parent) with short one proton (N) and atomic number (Z). The equation for Beta-decay is as follows:

$$^{A}_{Z}X_{N} \rightarrow {}^{A}_{Z-1}Y_{N+1} + e^{+} + \nu_e \, (+ e^{-}) \qquad (2.2)$$

Where X represent unstable nuclide, Y new nucleus and e^{-} stands for an ejected orbital electron so that the total charge can be balanced.

2.2.3 Initial energy and positron range

Initial energy is the energy possessed by a positron after being produced by beta decay. As positron travels through matter, it losses this energy and finally come to rest. Positron range is the term used to describe the distance travelled by a positron before it annihilates with an electron on its path. This range relies upon the emission energy of the positron and the electron density of the neighboring matter. Table 2.1 shows a list of the conventional radionuclides that emit positron and their properties.

Table 2.1: Properties of common positron emitting radionuclides used in PET (Cherry and Dahlbom, 2004)

Radionuclide	E_{max} (Mev)	Half-life	Mean positron range in water
^{13}N	1.20	9.97 min	1.4
^{11}C	0.961	20.4 min	1.1
^{18}F	0.63	109.8 min	1.0
^{15}O	1.73	2.03 min	1.5
^{68}Ga	1.89	67.6 min	1.7
^{82}Rb	2.60, 3.38	1.27 min	1.7

2.2.4 Annihilation photons, energy and non-collinearity

After positron is emitted from an unstable nucleus, it travels a little distance before it interacts with an electron on its path in a reaction known as annihilation. Two gamma photons emerge in opposite direction from such reaction, each with 511 keV (each particle's rest mass equivalent) (Figure 2.3).

Positron interaction with an electron could result to any of these forms, either they give two anti-parallel photons, or they form a positronium. Positronium comprises of a single positron and an electron orbiting at a central position of a system. There are two types of positronium, one is ortho-positronium in which the electron and positron spins are parallel and para-positronium where the spins are anti-parallel. Para-positronium decays further to give two anti-parallel 511 keV photons whereas ortho-positronium decays to emit three photons (Zaidi, 2000).

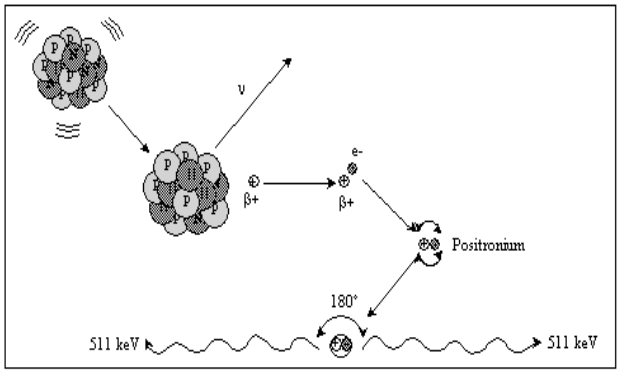

Figure 2.3: Schematic representation of positron emission and annihilation (Zaidi, 2000)

Non-collinearity (Figure 2.4) refers to the slight deviation of annihilation photons from the ideal direction by few tenth of degrees (usually +/- 0.25^{o} with an overall effect of 0.5^{o} on the FWHM). This often happens because the two back-to-back pair of photons are not just stationary rather they are moving at a particular velocity to reach the detectors. This distortion or non-collinearity gets greater with further distance travelled by the photons within the field-of-view of the scanner (Shukla & Utham, 2006).

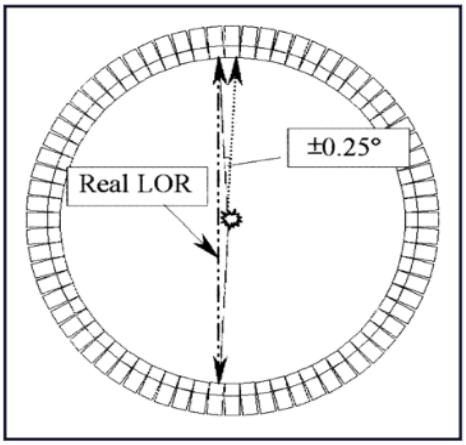

Figure 2.4: Schematic representation of non-collinearity (Shukla & Utham, 2006)

2.3 Photon Interaction with Matter

Photons of electromagnetic radiation undergo a certain form of processes as they pass through matter, which includes, some penetrating the matter without any interaction, some completely absorbed by the matter and some are scattered in several angles, with and without loss of energy. Contrary to photons of charged particles, those from positron-electron annihilation are known to be highly energetic, well-collimated and therefore they tend to be largely absorbed by matter. These nuclear medicine imaging photons are usually involved in three broad processes, namely; coherent (Rayleigh) scattering, photo-electric effect, and Campton (incoherent) scattering. Details are discussed below.

2.3.1 Rayleigh scattering

This is a form of scattering in which an entire atom becomes ionized by an incident photon unlike that seen in Compton scattering whereby only one electron becomes ionized. All the electrons in this atom move in the same direction as a result of the energy released from

the photon (Figure 2.5). Note: no electrons ejected from this interaction (Imagingkt, 2016).

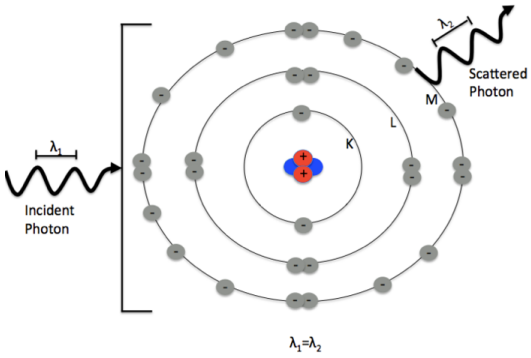

Figure 2.5: Schematic representation of Rayleigh scattering (Imagingkt, 2016)

2.3.2 The photoelectric effect

This is a type of photon-electron interactions that occur in an atom with the photon completely losing its energy, and subsequent ejection of electron from its shell. This effect is achieved when an incoming photon that is having an energy greater than the electron's binding energy, transfers its energy to the electron and removes it from its orbit (Figure 2.6). In this process, the photon is completely absorbed and the electron is now known to be photoelectron. This photoelectron receives energy equal to the energy of the incident photon minus the electron's binding energy. Three things are considered in photoelectric effect, namely; The incident photon's energy (E), Attenuating medium atomic number (Z) and Density of the attenuating medium.

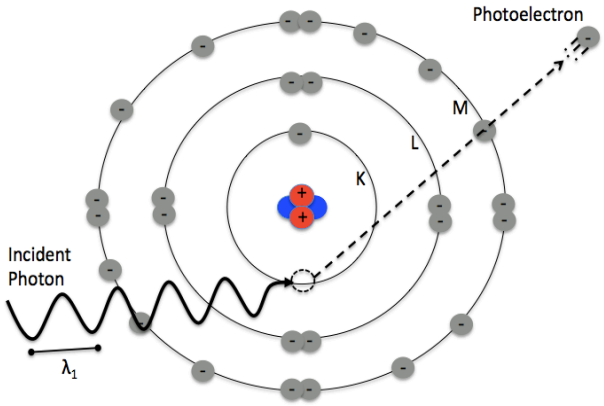

Figure 2.6: Schematic representation of photoelectric effect (Imagingkt, 2016)

A vacant space is left by the ejected electron which becomes occupied by a loosely bound outer electron (Figure 2.7). Such event leads to the emission of energy in the form of characteristic radiation, because each electron level has different binding energy (Radiologykey, 2016).

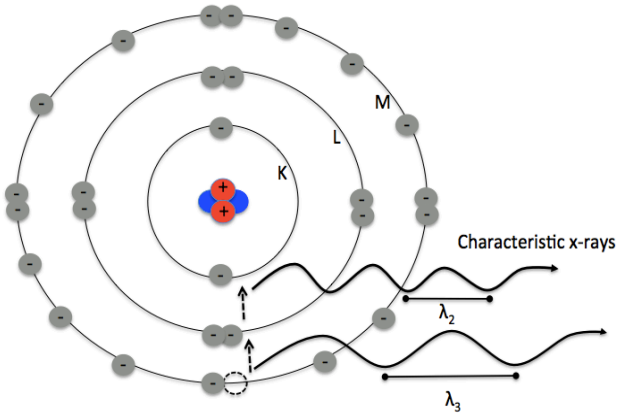

Figure 2.7: Photoelectric effect with X-ray emission (Imagingkt, 2016)

2.3.3 Compton scattering

In Compton interactions, a highly energetic incident photon hits and eject a free electron or loosely bound outer electrons (Figure 2.8). The incident photon changes direction (becomes scattered) and transfers energy to the ejected recoil electron. In this process, there is conservation of both energy and momentum because the scattered photon now has a different energy and wavelength. Note: the transferred energy depends on the number of electrons in the absorbing matter and doesn't depend on the absorbing medium's atomic number. The Compton equation is as follow;

$$E_{1=}\frac{E_0}{1+\left(\frac{E_0}{m_0c^2}\right)(1-\cos\theta)} \qquad (2.3)$$

where E_1 represents the scattered photon's energy, E_0 represents the incident photon's energy, m_0 represents the electron's rest mass energy, c^2 represents speed of light and cosθ represent the angle of scattering.

The incident photon's energy and the scattering angle determines the energy gained by the electron or that lost by the photon. As the scattering angle increases, more energy is

transferred to the electron. The maximum energy transferred by the photon is observed when the photon is scattered at an angle of 180 degrees (Radiologykey, 2016).

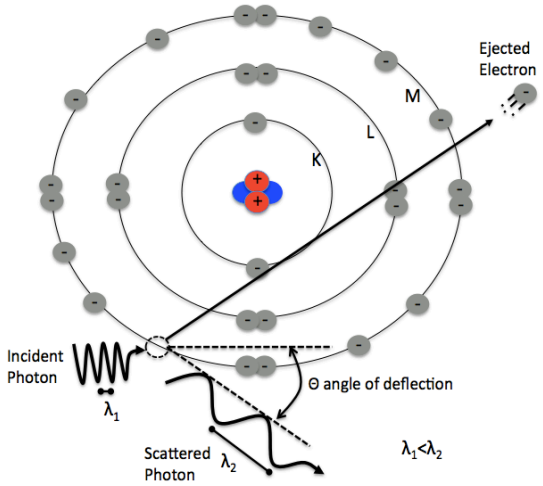

Figure 2.8: Schematic representation of Compton scattering (Imagingkt, 2016)

2.3.4 Pair production

Pair production involves interaction between an incident photon and the nucleus of an atom, alternatively with an orbital electron (in the case of triplet production). This interaction takes place with a high energy (typically greater than 1.02MeV) photon. This energy doubles the electron's rest mass energy, therefore, the interaction results in a transfer of energy to two charged particles, an electron and a positron (Figure 2.9). The energy absorbed by this charged particles is released through ionization and excitation. At rest, positron combines with an electron to produce two photons in opposite direction. These photons are important for nuclear imaging applications. Note: pair production does not occur in X-ray imaging due to the high energy required (Imagingkt, 2016).

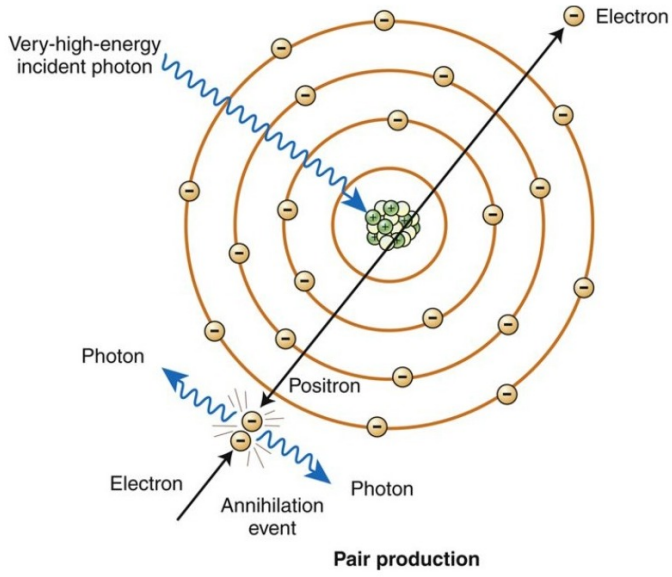

Figure 2.9: Schematic representation of pair production **(**Flickr, 2006)

2.4 Photo-detectors

These are sensing devices that responds to electromagnetic radiation for the purpose of detection and measurement. This is achieved when high energetic photon interacts with the surface of such devices. The main types of photo-detectors are; scintillator detectors, gas-filled detectors and semiconductor detectors. Photo detectors could be used for various purposes such as to measure photon energy, count incoming photons, measure position and arriving time of photons, and also for particle identification. A summary of the different types of photo-detectors is given below.

2.4.1 Gas-filled detectors

They are divided into three namely; Ionization chamber, Proportional counters, and Geiger-Muller counters.

Ionization chamber have been in use for several decades. It is a simple detector which utilizes the produced excitation and ionization of gas molecules when charged particles interact with gas. This photon-gas interaction creates several electron-ion pairs that move in random thermal motion. In the ionization chamber, some sort of collisions occurs between the ions, free electrons and neutral gas molecules. Such collisions include charge

transfer as a result of positive ion meeting a neutral molecule leading to the transfer of electron from the neutral molecule to the ion. Another type of collision is recombination, whereby the electron-ion pair try to recombine. This process is stopped by applying an electric field to separate the charge into electron and ion and collecting them on the positive and negative electrode. With strong electric field, all the charges can be collected without loss. Lastly, an electric current called ionization current is measured through. This is the basic principle of DC ion chamber. A simple example of ion chamber is a capacitor with a gas dielectric (Figure 2.10). Inert gas such as argon and xenon are often used to prevent chemical reactions within the gas after ionization.

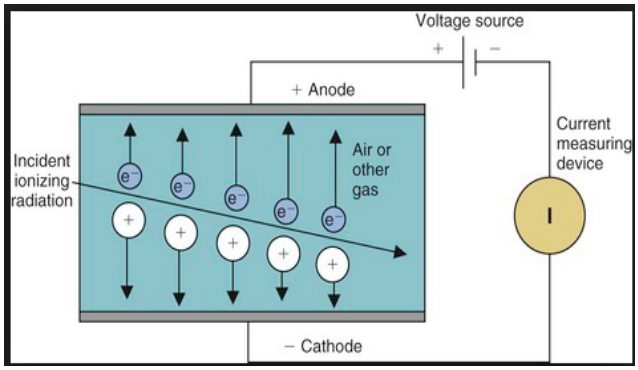

Figure 2.10: Basic principle of gas-filled detectors (Radiologykey, 2016)

When ionizing radiation comes in contact with the gas molecules, electron-ion pair are created. A sufficient electric field is needed to distribute this charges to the plates of the capacitor with the positive plate attracting the electron and negative plate attracting the ion. In the absence of sufficient electric field, a recombination of the charges is likely to occur.
Ion chambers can function in current mode or pulse mode. While operating in current mode, electrons can be obtained as either free electrons or negative ions. Therefore, any filling gas such as air could be used to operate the ion chamber. Whereas pulse mode applications are very limited but sometimes it can be used for fast neutron spectrometry. Ion chamber applications include measurement of gamma ray exposure (Kamal, 2014).
Proportional counters function just like ionization chambers but requires strong electric field. It uses a process called gas multiplication to produce large voltage by multiplying the number of ions produced. The presence of strong electric field makes electrons to have

high kinetic energy and therefore can ionize neutral molecules, whereas the ion counterpart gets little energy and low mobility between collision. These pair of electrons are then accelerated to cause further ionizations. The whole of the process takes a cascade form known as Townsend avalanche (Figure 2.11). It is to be noted that in proportional counters, the number of electrons is exponentially increased with distance. These counters are mostly used to differentiate between particle detection and radiation dose measurement. Low efficiency is a major disadvantage of this counters (Kamal, 2014).

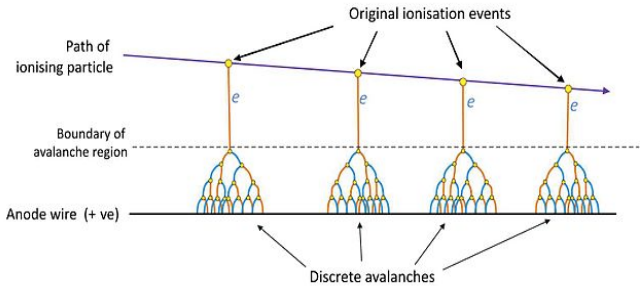

Figure 2.11: Avalanches in proportional counters ("Wikiwand", 2017)

Geiger-Muller counters are similar to proportional counters but they utilize an electric field strength greater that used by proportional counters. Exponential number of avalanches are produced by these counters which makes them to be used strictly for radiation counting and not for spectroscopy. There is lost of records for the amount of deposited energy by the incident radiation in this counters. Geiger counters are simple and economical radiation counters because they are of low cost and are simple to operate. Their main disadvantage is large dead time, and also they cannot separate between the time of radiation detection and the energy of the detected radiation. In Townsend avalanche, the excited gas molecules emit photons when they return to their ground state. These photons are likely to be absorbed by the cathode wall or other gas molecules through photoelectric effect. Free electron is created in this process, the electric field inside the detector accelerates this new electron and causes another avalanche. By so doing, Geiger discharge is created (Figure 2.12) leading to a formation of many avalanches throughout the multiplying region that surrounds the anode (Kamal, 2014).

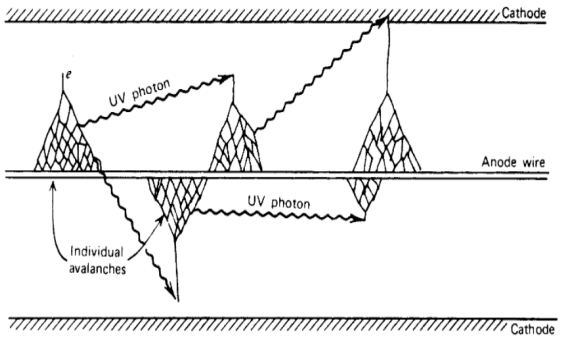

Figure 2.12: Schematic representation of Geiger discharge ("Wikiwand", 2017)

2.4.2 Scintillator detectors

Scintillator detectors are the most widely used radiation detection materials in present day technology. These materials work on the principle of luminescence, a phenomenon whereby a material emits light after being struck by an incoming radiation. The architecture of scintillator detectors (Figure 2.13) is made in such a way that the crystal is attached to a photo sensor (photo-multiplier tubes (PMT) or photo diodes). Incident photons when in contact with the scintillator crystals transfers its energy to the crystal, the crystals absorb the energy and emit it in form of light which is detected by a photosensor attached to the crystal. This light which becomes converted into photoelectrons by the photo-sensors is then amplified at varying potential difference within the photo-sensor and later collected at the anode part of a photo-detector where it becomes transformed into an electric signal (Niki, 2006).

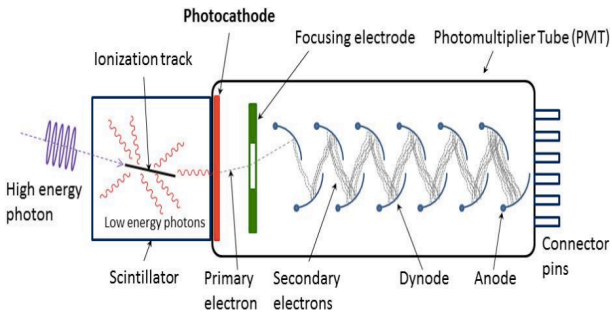

Figure 2.13: Scintillator detector with a scintillation material coupled to a PMT ("Scintillation counter", 2017)

Characteristics of scintillator detectors are as follows:

- Conversion efficiency
- Stopping power

- Light output
- Decay time
- Energy resolution
- Linearity

Conversion efficiency: The amount of charged particles converted to light with respect to the absorbed energy of the charged particle. High conversion efficiency is preferred for fast and superior resolution imaging.

Stopping power: Is the ability of the scintillator crystal to attenuate more of the incident photon. It is linearly related to the density and the atomic number of the scintillator crystal. High stopping power is required for good image resolution.

Light output: Number of photons emitted with respect to the energy absorbed by the scintillators. High light output gives good spatial resolution. Light output is linearly related to conversion efficiency of the scintillator material and also to the energy and type of incident photon.

Decay time: Time interval between excitation and decay back to initial state of the atom within the scintillator material that leads to the emission of light. Short decay time is preferred because it makes the detector to handle more event rate. Furthermore, fast decay time enhances fast light production for a better timing resolution.

Energy resolution: This is an intrinsic property of a detector material which gives it the ability to measure the energy of the deposited particle and also to differentiate between radiations of varying energies.

Linearity: This is the ability of the material to give out light equivalent to the charged particle's deposited energy.

Other qualities to be considered are fast operation speed, low cost, non-hygroscopy and durability. Scintillation materials are classified into organic and inorganic materials. Inorganic materials often require an additional dopant such as thallium (Tl) or cerium (Ce) that produce the scintillation light. The inorganic group are characterized with high densities, high stopping power, high effective atomic number and high conversion efficiency for electrons or photons and are therefore the preferred detectors in nuclear imaging applications (Niki, 2006). Example of inorganic materials are; $Lu2Y_2SiO5$: Ce

(lutetium yttrium oxyorthosilicate doped with cerium), Lu_2SiO_5: Ce (lutetium oxyorthosilicate doped with cerium), NaI:Tl (thallium doped sodium iodide), $Bi_4Ge_3O_{12}$ (bismuth germanate), Gd_2SiO_5: Ce (gadolinium oxyorthosilicate doped with cerium) and BaF2 (barium Fluoride). Properties of scintillator material is shown in Table 2.2. Low energy resolution is the major disadvantage of scintillator detectors.

Table 2.2: Properties of scintillator crystals (Junwei et al., 2009)

Properties	**NaI(Tl)**	**BGO**	**GSO**	**LuAP**	**LSO**	**LYSO**
Effective atomic no. (Z)	71	74	59	65	66	60
Attenuation coeff. (cm^{-1})	0.34	0.92	0.62	0.9	0.87	0.86
Density (g/cm^{-3})	3.67	7.13	6.7	8.34	7.4	7.1
Index of refraction	1.85	2.15	1.85	1.95	1.82	1.81
Light output	100	15	30	16	75	75
Peak wavelength(nm)	410	480	430	365	420	420
Decay time (ns)	230	300	65	18	40	41
Hydroscopic	Yes	No	No	No	No	No

2.4.3 Semiconductor detectors

These detectors work base on the same principle as gas-filled detectors. The basic working principle of this detectors is ionization process which occurs as a result of the interaction between the incident photon and the detector material. The interaction causes absorption of photons by the detector material leading to excitation of the valence band electrons. These electrons move to the conduction band, and the valance band is left with an electron-hole pair. As detector material absorbs more energy, an increasing number of electron pairs is created in the valence band of the detector (Knoll, 2010). A Large number of charges are available because of the incident photon's absorbed energy. These charges need be separated and distributed onto the electrodes of the material so that recombination is prevented. Separation is achieved by applying an electric field usually generated by the electrodes of the material. An electric signal is produced afterward which becomes translated by linked electronics (Cherry, 2004).

Two types of semiconductors are available, a N-type and P-type (Figure 2.14). In the N-type, the materials (Si or Ge) which has 4 valence electrons, are doped with group 5 atoms like Boron (B) or Gallium (Ga). As a result, 5 valence electron are added to the material lattice, of which 4 will be accommodated and one excess electron will be left. The excess electron serves as a negative charge carrier. In the P-type, the materials are doped with group 3 element, this causes a change in the electron-hole. The dopant donates only 3 valence electron, hence leaving one excess hole. The hole is regarded as positive charge carrier. A p-n junction is formed when the two semiconductor materials are joined. In-between the charge carrier is a neutral region (depletion zone) that serve as the active region in semiconductor detectors.

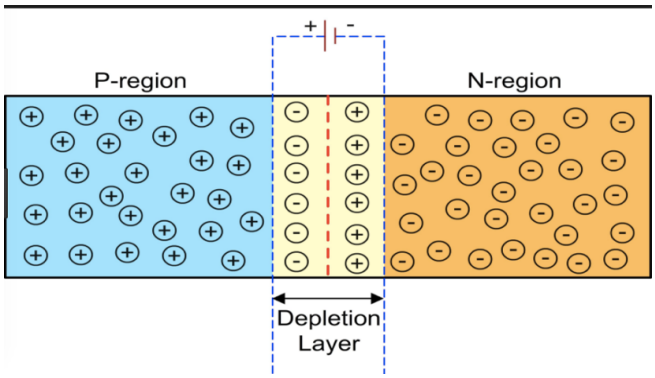

Figure 2.14: Schematic representation of a P-N junction (Cherry, 2004)

An electric field could also be created by reverse bias voltage across the detector, this causes a change in position of the charge carriers in the depletion zone (holes drift from p to n and electron does otherwise). Presence of photons in the material accelerates electrons to the n-region and holes to the p-region, by so doing, an electric field is generated spontaneously.

Semiconductor materials have some known problems which are often created by the bias voltage. They include polarization effect, current leakage and charge trapping (arising from crystal impurities). The major disadvantage of these detectors is low stopping power for 511keV photons and cost. On the other hand, they have good energy resolution (1-4%). For photon detection purpose, the below listed are the most commonly used semiconductor materials with their properties given in Table 2.3.

- Silicon (Si)
- Germanium (Ge)
- Cadmium telluride (CdTe)
- Cadmium zinc telluride (CZT)

Table 2.3: Properties of semiconductor materials (Takahashi and Watanabe, 2000)

Property	**Si**	**Ge**	**CdTe**	**CZT**
Atomic no. (Z)	14	32	48/52	48/30/52
Density (g/cm^3)	2.33	5.33	5.85	5.81
Band gap at 300K (eV)	1.12	0.663	1.44	1.6
Energy resolution (% at 511keV)	0.1-0.3	0.1-0.3	1	2-3
Electron mobility (cm^2/Vs)	1400	3900	1100	1000
Hole mobility (cm^2/Vs)	450	1900	100	50

2.4.4 Comparison between solid state and scintillator crystals

Solid state crystals:

- They have excellent energy resolution (Avg. 1%)
- They have low atomic number and density ($5.85g/cm^3$), leading to their low quantum detection efficiency for 511keV photons
- They are very expensive

Scintillating crystals

- They have high quantum detection efficiency which is as a result of their large atomic number and density
- They have high light output
- They have fast decay time (short life time of fluorescence)
- They have poor energy resolution (Avg. 10-14%) or higher

- They have good timing resolution
- They are very cheap
- They have high counting rate capabilities

CHAPTER 3
OVERVIEW OF PET IMAGING TECHNIQUE AND PET IN NUCLEAR MEDICINE

3.1 Annihilation Coincidence Detection

PET is a nuclear imaging technique which involves the use of radiopharmaceutical to provide functional images of the living tissue. A radio-tracer, typically ^{18}F-fluoro-2-deoxy-D-glucose (FDG) is injected into the blood stream, where it travels in the blood stream and by the tissues and cancerous cells. Tumors have higher affinity for glucose than normal healthy cell, therefore they tend to absorb more of the radiotracer. The working principle of PET is based on annihilation coincidence detection, which occurs when the injected radiotracer is subjected to beta-decay and emits a positron (e^+). Positron annihilates mutually with an atomic electron (e^-) to form a positronium which decays and emit a pair of back-to-back 511 keV gamma rays at nearly 180 degrees. These photons are the by-product of the converted rest mass of both positron and electron (Figure 3.1). Prior to annihilation with an electron, the positron travels a small distance (a few mm) depending on its range and energy. The origin of the photons is identified along a line between the PET detectors via simultaneous detections of the two photons. This makes it possible for PET detectors to locate the point where the photons are coming from without the need of a collimator (Cherry, 2012).

The PET scanner is basically a ring of photon detectors surrounding a patient, and it comes with some exclusive integrated circuits that gives it the ability to recognize pairs of annihilation photons. Coincidence detection of a pair of photon by two opposing PET detectors signifies that a decay event happened on a straight line between these detectors. Information obtained from the PET detectors is archived in a computer system inform of sinograms. These sinograms are used to reconstruct positron emitter distribution in 3D format which results to a set of tomographic images (Mikhaylova, 2014).

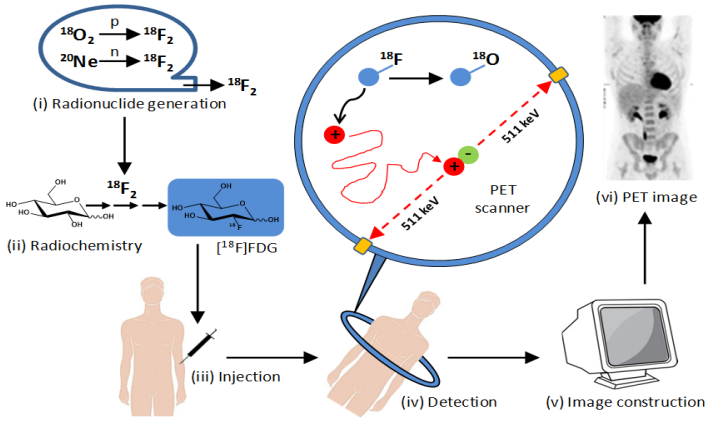

Figure 3.1: PET working principle (Patching, 2015)

3.2 Radiopharmaceuticals in PET

Pharmaceutical refers to any chemical substance designed to be use for diagnosis, treatment, and or prevention of diseases. Radiopharmaceuticals are pharmaceuticals tagged with a radionuclide. In nuclear imaging, these radiopharmaceuticals are used as tracers for the purpose of diagnosis and treatment of several disease conditions. Several tracers are employed in a variety of biochemical, pharmacological and biophysical pharmacological processes in the living organism. Clinical areas to which such tracers are used include; neuroscience cardiology and oncology. Nevertheless, tracers to be used for PET imaging need to meet up with certain criteria such as; high specific activity. The specific activity refers to the reduction in activity of a radionuclide, when a radiopharmaceutical is undergoing chemical synthesis.

Furthermore, tagging of radiopharmaceuticals with radionuclides that has adequate half-life sufficient to examine the selected biologic process, and expectedly to last the same period as the radiopharmaceutical's biological half-life is encouraged. Biologic half-life refers to the time in which the radiopharmaceutical completely leaves the body. Radiopharmaceuticals have different uptake and clearance manners; some their uptake is fast while that of others is slow. Some leave the body earlier while others take longer time. The radionuclide's biologic half-life and physical half-life decides the quantity radioactive decays produced in an area with respect to time. Thus, both parameters ought to be considered when setting the patient radiation dosage. Lastly, Non-toxic radiopharmaceuticals are required so that the patients won't be poisoned.

All radioisotopes from Table 2.1 are used in PET. Another factor to consider when choosing positron emitters for PET exams is the mean energy. Large positron range makes annihilation to occur at a large distance from decay event and this worsens the system's spatial resolution. Radionuclides with short half-life require a cyclotron within the PET environment, whereas those having long half-life present issues regarding disposal and storage. PET radionuclides are required to have physical and chemical properties that makes them suitable for metabolic studies.

Positron emitters like oxygen (^{15}O), nitrogen (^{13}N), and carbon (^{11}C) allow labelling of several organic molecules and this makes them good for use in PET. However, the complexity of the labelled molecules is reduced because of their short half-lives. Likewise, a lot of in- vivo studies is limited with such positron emitters. Another group of positron emitters appropriate for complicated labelling and longstanding biological changes exam due to their relative long half-lives include ^{76}Br with $t_{1/2}$ of 16 hours, or ^{124}I with $t_{1/2}$ of 4.2 days.

Flourine-18 (^{18}F, see Table 2.1) happens to be an exception because a great success has been achieved following its use in PET. It has a short positron range which allows it to fit into PET scanners with sub-millimetre spatial resolution. Moreover, its long half-life makes it to be distributed few hundred kilometres away from the production site, rendering cyclotrons needless in the hospitals. FDG is absorbed by cells with high affinity for sugar like cancer cells, kidney, and brain. Among the existing radiopharmaceuticals, it is the most effective one. It is a single tracer with varieties of use such as in brain metabolism study, cardiac function, and cancer detection (Mikhaylova, 2014).

3.3 Acquisition Modes

This section talks about the forms of data acquisition in a PET scanner. The previous section mentioned that PET imaging relies of annihilation coincidence detection of two 511keV gamma photons. There are three ways in which the detected events can be acquired namely: the list mode, frame mode and gated imaging. Different coincidence logics are used in each scanner operation mode.

In list-mode acquisition, there is digitization of information regarding detected events. But sorting of this information into an image grid doesn't occur immediately. The information

comprises of energy, coordinates, arriving time of individual event etc. Additional information could be possibly added such as patient movement or position. In this mode data acquisition occurs prior to the coincidence searching and retrospective framing is allowed. In data analysis, this method provides greater simplicity. Nevertheless, it lacks adequate memory usage for conventional imaging acquisition.

For frame-mode acquisition, position signals of individual events are digitized followed by sorting into the right x-y locations inside the digital image matrix. The image data acquisition is halted and the pixel values are saved in the computer storage following an elapsed preset time or following a preset recorded number of counts. A frame refers to an individual image obtained is a series of sequences. Prior to the acquisition process, the image matrix size must be specified.

For gate imaging mode, information is gained simultaneously with the respiratory cycle or pulse. By so-doing, all images are obtained in the meantime amid the movement cycle (Cradduck and Busemann-Sokole, 1985).

3.4 Two-Dimensional (2-D) and Three- Dimensional (3-D) Data Acquisition

2-D data acquisition simply describes a method which is controlled by the action of a septa on the incoming photons. Right from the beginning of its introduction into nuclear medicine, PET designs are made in such a way to accommodate collimators of tungsten or lead materials between detector rings. Presence of such collimators makes incoming photons parallel to the detector to be detected and scattered photons becomes attenuated by the collimator. The septa are also known to minimize single-channel counting rate, as a result random rate are lowered with the true coincidence left to be recorded. The sensitivity of 2-D acquisition can be improved by connecting pairs of detectors in two adjacent rings in a coincidence circuit.

3-D acquisitions were introduced to improve the sensitivity of PET scanners which was achieved by eliminating the collimators, and acquisition occurs via line of responses (LOR). Compared to 2-D mode, 3-D leads to an increase in sensitivity by a factor of 4 and above. The sensitivity in 3-D mode happens to be high at the center than at the periphery. Full 3-D reconstruction are also done for images from 3-D acquisition mode. Lastly, due to

the high sensitivity observed in the 3-D mode, it has now become globally used in state-of-the-art PET systems (Lodge et al., 2006).

3.5 Classification of Detected Events

A valid event must satisfy the following conditions;

- A pair of photon is detected within an established coincidence time window.
- The formed LOR by both photons should be inside a valid acceptance angle of the system.
- The photon energy deposited on the crystal falls inside the chosen energy window.

Events which meet up with the above-mentioned conditions are called prompt events (or "prompts"). Nevertheless, due to photon scattering or coincidence arising from random detection of photon pairs of unrelated annihilation, some of the prompt events become undesired events (Bailey et al., 2005).

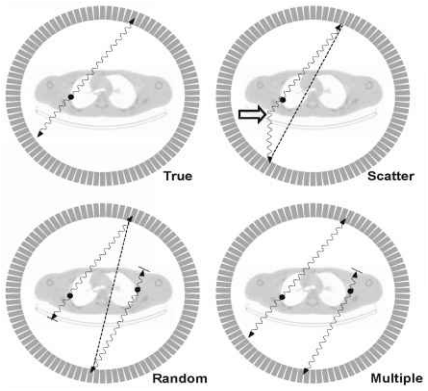

Figure 3.2: Detected events in PET. Dotted lines in the scatter and random events indicate miss-assigned LOR (Bailey et al., 2005)

Description of terms used in PET detected events

True coincidence: This type of event occurs when both annihilated photons coming from the same event arrive at the opposing detectors in a specified time window.

Random coincidence: This event occurs when two different annihilation takes place, giving rise to four photons of which only two (one from each annihilation) are able to arrive the detector and be identified as if they are from the same annihilation. The other

two photons are lost. Image artefact and contrast depreciation are noticed when a random event occur.

Multiple (or triple): This involves the detection of three events arising from two annihilations. It often occurs at high count rate whereby more than one detector becomes activated. Multiple events are usually not considered because you can't tell the photons arising from same annihilation.

Scattered events: This usually occur when one or both photons undergoes Compton scattering before being detected. The scattering is often due to a weak photon energy (less than 511 keV). As a result, a false line of response is assigned between the detectors which doesn't correspond to the origin of the annihilation. Causes of scattering include the gantry, patient, and the detector.

3.6 Reconstruction Techniques in Tomographic Imaging

3.6.1 Line of response, projections, and sinograms

Line of response (LOR): This is a line that connects two detectors involved in a coincidence detection of annihilation photons. This line gives an idea of the point where an event took place.

Projection: This is defined as a group of lines of response registered over a detector at a certain angle.

Sinograms: Matrix of projections from several angles. The word sinogram originate from the sine curve shape produced by a point source object placed in a particular position (Figure 3.3).

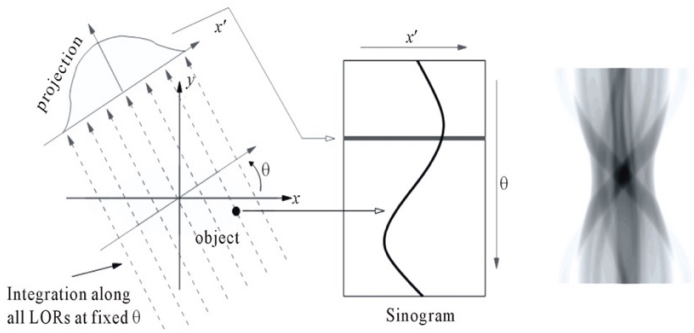

Figure 3.3: 2-D display of projection sets called sinogram (Asl & Sadremomtaz, 2013)

PET coincidence events are often saved as sinogram. These sinograms form the background of image reconstruction in medical imaging.

The combination of PET systems with image reconstruction algorithms are the reason for their success in nuclear imaging, following the production of a 3-D map of radiotracer distribution within the patient. The 3-D images obtained from PET is formed from stacked 2-D reconstructed sections of the object. This image acquisition pattern is termed as tomographic imaging.

Several image reconstruction algorithms exist, which are either analytic or iterative methods. They include Filtered backprojection (FBP), Maximum-likelihood expectation-maximization (ML-EM) algorithm, Ordered subset expectation maximization (OSEM), List-mode OSEM (LM-OSEM), and Origin ensemble (OE) algorithms. A brief explanation of these algorithms is given below.

3.6.2 Filtered back projection (FBP)

This is a very fast image reconstruction method due to its analytic nature. It is easy to use in the control of noise correlations and spatial resolution in the reconstruction. It employs projection slice theorem in combination to back projection, in such a way to eliminate image blurring. It works like Fourier transformation but with an addition of a ramp filter before performing the conventional back-projection. The FBP is designed to overcome the limitation of conventional back projection method (Maligs, 2017). The basic steps are shown in Figure 3.4.

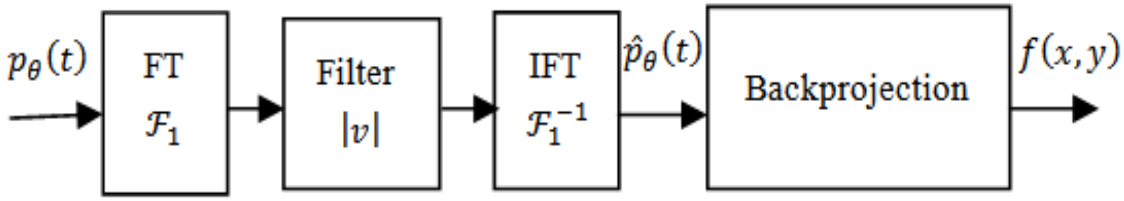

Figure 3.4: FBP concept (Maligs, 2017)

Where Pθ represent the detector function, and is the projection measured along all lines of response at an angle θ. *f(x,y)* represent a 2D object which is defined by the function *(f)*.

First, the image undergoes 1-D Fourier transform (FT), so that filter can be applied to the FT profile. The next step is to compute the inverse FT of each FT profile, by so doing

filtered projection profiles are acquired. Lastly, using the filtered profiles, a back projection is performed (Kinahan, Defrise, and Clackdoyle, 2004).

3.6.3 Ordered subset expectation maximization and maximum likelihood expectation maximization (OSEM and MLEM)

These methods are being employed into medical imaging field due to the mass improvement in the processing speed of computer systems. Advantages of such methods include minimized sensitivity to detector imperfections.

The methods involve making an initial image estimate, e.g a uniform or blank image followed by computation of projections from the image estimate via a process known as forward projection. To achieve this, the intensities along the path of the photons is summed for all the projections through the estimated image. Later on, a comparison is made between the measured and estimated projections. If any difference is observed, then corrections are made to upgrade the estimated image. Convergence between the two projections is evaluated by performing a new iteration. The whole step is repeated several times and solution is achieved through image estimate convergence. Both methods have a lot of similarities and they are the most widely used image reconstruction techniques nowadays.

OSEM was introduced to reduce the reconstruction time of MLEM. It uses subsets of the complete set of data for every image update. Non-overlapping subset is one of the approach it uses to divide the projection space into subsets. Out of all the subsets, only the projections in a single subset are summed by the back projection steps. Therefore, image update is done after each subiteration. When only one iteration is done, then OSEM is exactly the same as ML-EM (Alessio and Kinahan, 2006).

MLEM is mostly applied to solve incomplete data problems. It is very effective in finding the maximum likelihood estimate. Although this method has advantages like predictable and consistent convergence manner, it also has drawbacks like very noisy images. To solve this, the algorithm is stopped before convergence. In addition to the previous solution, noise suppression is done by smooth filter application on the reconstructed image. The second drawback is its slow convergence. It typically requires many iterations. When compared to FBP, MLEM takes more computation time (Tong et al., 2010).

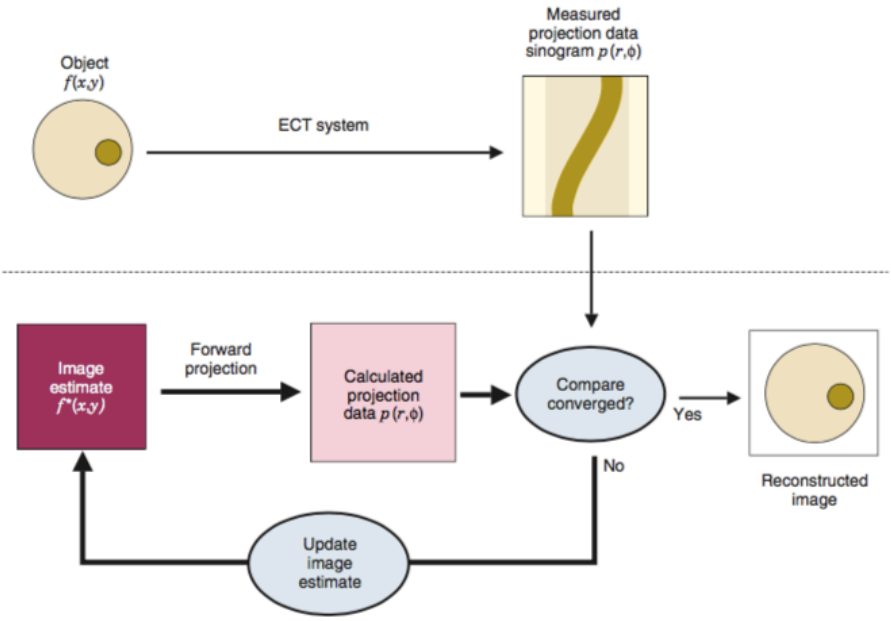

Figure 3.5: Schematic illustration of the steps in iterative reconstruction (Cherry, 2012)

3.6.4 Origin ensemble (OE)

This method is fast converging and its execution is straightforward. It doesn't depend on the number of channels. The initial step involves assigning a random position on the LOR of each event and at each FOV voxel location, the density matrix saves the number of events. During iteration, each event undergoes several steps such as; assigning a new location, accepting the new location with a probability P, and lastly comparing the density at the new location with that at the old. The density matrix is updated immediately when a new event position is accepted, prior to the next event. Several trial runs have to be run because of the stochastic nature of the algorithm and the mean of the trial runs is considered as the final result (Kolstein et al., 2013).

3.6.5 List mode-ordered subset expectation maximization (LM-OSEM)

List-mode (LM) is similar to OSEM only that it uses list mode format of data presentation. There is a replacement of detector bins by detected events in the iterative update function. Nevertheless, because of the numerous pixels in the scanner FOV which are likely to contribute to a specific detected event, this method results in slow convergence and also consume a lot of time (Kolstein et al., 2013).

3.7 Parameters affecting Image Quality

Image quality is the term referring to the accuracy of a reconstructed image of an object with respect to the original object being imaged. Features include:

- Spatial resolution
- Image contrast
- Image noise

Spatial resolution: The ability to differentiate between two closely related objects. It is also related to the number of pixels used to produce a digital image given rise to a sharp image.
Image contrast: This is the intensity variations between areas of an imaged object that has different radioactive uptake.
Image noise: This could be described as the random statistical variations in counting rate, that lead to a spotty appearance on the final image (random noise) or the non-random variations in counting rate that overlap on and obstruct the structures of the object of interest (structured noise).
Factors contributing to the final image quality will be classified into three broad groups: Detector related limitations, intrinsic limitations, and limitations from other sources. Below is a brief review of the above-mentioned factors.

3.7.1 Limitations accompanying detectors

3.7.1.1 Spatial resolution

This can be improved by reducing the pixel size of the elements. An error R_{det} often observed at the center of the detector is d/2 whereas at the edge is d. Therefore, the SR is greatest at the CFOV and slightly decreases towards the periphery. A very fine detector pixelation is needed for good SR to be achieved.
Another detector-related error is parallax or depth-of-interaction effect (DOI). The DOI tells us the exact point of photon-detector interaction (exact point of energy deposition). This type of error occurs when a photon enters the detector element at a slight oblique angle leading to a mismatch between the true and measured line of response because the exact position of interaction is unknown. This effect is mostly noticed in detectors where the distance between opposing detector elements is very small like organ dedicated

scanners or where the annihilation occurs very close to the edge of PET in a circular geometry. Figure 3.6 shows depth of interaction effect. The error become worsen with increasing depth of individual detector, thus the error is minimized using thin crystal with high stopping power (Braem et al., 2004). PET systems with larger diameter are less likely to have parallax error compared to organ dedicated systems, because the photons from annihilation will be more on the central region with less oblique deviation.

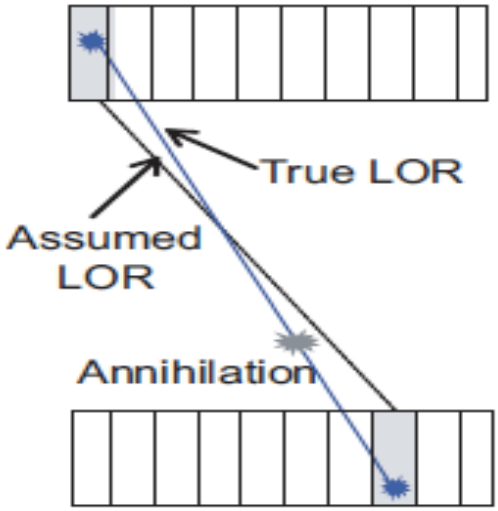

Figure 3.6: Depth of interaction effect (Martins, 2015)

3.7.2 Physics related limitations

3.7.2.1 Spatial resolution

Here, finite positron range is a contributing factor to the limitations of image quality produced by PET systems. The positron range relies on two factors, its energy of emission and the composition of neighboring matter. These two factors make it present some uncertainties with regards to the position where the nuclide decay takes place, leading to a reduction in spatial resolution (Levin et al., 1999). The greatest distance covered by a positron without being scattered and moves on a straight path till the end of its range is known as Actual positron range whereas the mean distance covered from the emitting nucleus to the end of the positron range is known as Effective positron range (R_p) (Figure 3.7). Annihilation photons non-collinearity is another limitation, which is as a result of the remaining energy of the positron at the time of annihilation. This non-collinearity adds up

to the uncertainty in locating the annihilation point and therefore, reduce the system's spatial resolution. This effect is most noticeable in systems with larger diameter.

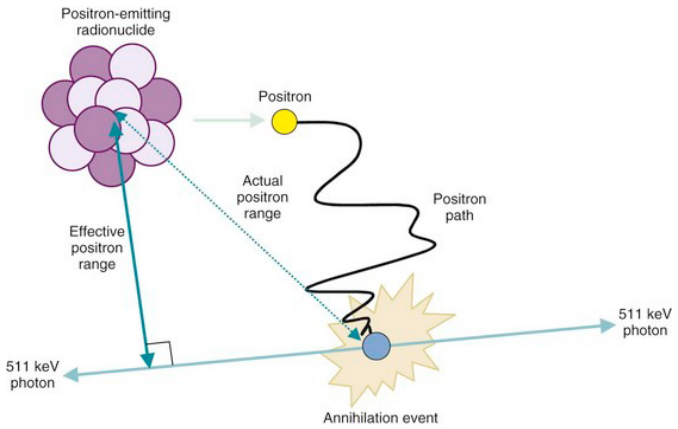

Figure 3.7: Effective and actual positron range ("Positron emission tomography", 2017)

3.7.3 Limitations from other sources

3.7.3.1 Spatial resolution

Factors such as patient motion, reconstruction method, and pixelization effect in the image worsen the system's spatial resolution. The filters used in image reconstruction sometimes results in further degradation of the spatial resolution. Patient motion which include cardiac or breathing-related also affects the final image sharpness. In order to minimize blurring caused by respiratory motion, mechanisms such as breath-holding and special breathing techniques are used. Sometimes, little of patient motion can be solved via special correction algorithms. Pixelation effect usually occur on the reconstruction image, whereby the resolution of the image is being affected by the size of the pixels used to create the image. In a situation whereby the pixel size happens to be larger than 1/3 of the expected system's spatial resolution, then the image will suffer from loss of details. It should be worthy of note that, smaller pixel size lead to high signal-to-noise ratio (SNR) of the individual pixel.

3.7.3.2 Contrast

High contrast images are being influenced by radiopharmaceutical with high lesion-to-background uptake. Factors like background counting rates which results from sources like

random, multiple and scatter could limit the contrast. Contrast is also affected by the number of count density (number of collected coincidences). A noise is usually observed in the image when the count density is small, therefore in order to obtain excellent image contrast certain number of counts must be reached. The required number of coincidences is determined by the organ uptake, dose of radiopharmaceutical administered, the scanner's quantum detection efficiency and the screening time. Another factor that can affect the image contrast is the lesion size with respect to the neighboring tissue and system's spatial resolution. To be more specific, it takes into account if an activity exists in the lesion (hot) or not (cold). Cold lesions often disappear in higher activity background tissues whereas hot lesions receive high contrast relative to low background.

3.7.3.3 Image noise

Image noise results from varying pixel counts across the image. Most of the parameters affecting the image contrast, affects image noise as well. They include background counting rate and non-uniformity of the imaging system. Increasing the number of total counts in the image is a good solution. But in order to achieve this, certain things need to be done including the use of longer scan time, use of high quantity of radiopharmaceutical and improving the detection efficiency of the scanner. These solutions can affect the patient in a negative way, and can also increase the dead time losses and random coincidence. Therefore, they are not preferred. Noise can be minimized by increasing the noise equivalent count rate (NECR). Noise level assessment can be done by calculating the SNR or contrast-to-noise ratio (CNR. Noise can also arise from the imaging procedure or from the imaging device. For example, an uptake by a particular organ may obscure the lesions in tissues close to it. Artifacts from image reconstruction could also appear as noise in the final image.

3.8 Image Artifacts and Corrective Measures

Photons undergo certain processes such as compton scattering, photoelectric interaction, pair production, and Rayleigh as they pass through matter and these effects need to be corrected when reconstructing high quality images.

3.8.1 Data normalization

This simply refers to the correction of effects arising from spectral non-uniformities and detector efficiency. Certain factors including detector sensitivity usually varies in a PET scanner. This happens because photons are emitted at different incidence angle, and the detecting medium size varies. Therefore, a non-uniformity in the obtained raw data exist (Badawi and Marsden, 1999). Normalization can simply be achieved by subjecting all detector pairs to same radiation source and recording the number of counts registered by each detector pair. In order to perform this, a blank scan can be done with a source made of water placed inside the FOV of the scanner, and collecting data in either 2D or 3D modes.

3.8.2 Attenuation correction

Attenuation of photons in tissue is one factor that minimizes image quality and the measured effectivity of PET systems (Zaidi and Hasegawa, 2003). Therefore, attenuation corrections need to be done. Photons emerging from the central region of an object happens to be more attenuated than those coming from the periphery of that same object. Non-uniformities from such process is observed due to the reason that most of the coincidence events coming from the center of the object are lost. Thus, a correction is needed for the photon attenuation in that tissue. Methods of attenuation correction include Chang's multiplicative and transmission method (Zaidi and Hasegawa, 2003).

3.8.3 Random coincidences correction

Random coincidences cause artifacts on the final image. Parameters like increased coincidence time window, energy window width and activity makes the random coincidence to increase. Reducing the coincidence time window could help reduce the random coincidences. Yet, such window need to be wide enough in order to accommodate the true coincidences because of the variations in arrival times. Therefore, there is a compromise between minimizing loss of sensitivity for true coincidence and minimizing the acceptance of random coincidences. Methods for random corrections include delayed window method. For dual-head coincidence (DHC) cameras, an alternative method is detector shielding from activity lying outside the FOV of the scanner (Sossi et al., 2000).

3.8.4 Correction for scattered coincidence

Scattering affects, the quality of an image via producing a fog background on the reconstructed image, mostly seen on the central region of the image. Scattering is influenced by the depth and density of body tissue, the activity within the patient, the energy window width and the density of the detecting material of the PET scanner. PET systems usually have high scatter fraction ranging from 10-15% and even up to 40%, mostly seen in 3D mode of scanning where no septa are used. In order to correct for the scatters, a method which involves taking the counts outside the FOV where no true coincidences are expected is employed. The outside counts take in both scattered and randoms, therefore, scattering counts will be left after correcting for randoms. Afterwards, signal intensity is measured and fit to 1-D Gaussian to obtain the corrected image (Cherry and Huang, 1995).

3.8.5 Dead time losses correction and pile-up

The pulse pile-up events refer to a situation whereby the energies of two or more photons get summed when they arrive concurrently. Should these events undergo compton scattering, their resultant peak is likely to be within the energy acceptance window. These two unrelated events make the event to be counted but wrongly positioned. Image distortion is caused by high count rates and pile-up events.

The dead time refers to a time in which a second event cannot be registered and processed by the PET system, thus it becomes a lost event (Knoll, 2010). Pile-up and dead time effects completely eliminates the relationship between registered coincidence events and the total activity within the FOV. Therefore, at high count rate, there will be a minimized radioactivity concentration.

Sources of dead time include integration time, analogue to digital conversion time and data transmission speed (Bailey et al., 2005).

3.8.6 Image artifact: partial-volume effect

Small structures and regions are usually faced with a diminishing activity due to the limit in spatial resolution of imaging systems. This condition happens in medical imaging particularly in PET and SPECT. In a situation whereby the region or structure to be imaged

is smaller than twice the FWHM resolution in the X-Y- and Z- dimension of the imaging system, the apparent activity of such region or object becomes lower. Systems with higher resolution are able to minimize this effect because they resolve the tissues excellently. This loss of activity arising from the scanners is known as partial-volume effect (Hoffman, Huang & Phelps, 1979). This effect leads to a reduction in contrast among high and low uptake regions.

Recovery coefficient (RC) can be applied to eliminate the partial volume effect. Sometimes, an effect called spill over is noticed in certain scenarios in which an object of interest contains an activity that is low compared to the neighboring structures. The activity from the surrounding structures then spill over onto the object of interest.

3.8.7 Reconstruction related image artifacts

The traditional image reconstruction method (FBP) also creates some artifacts. Conditions such as wrongly choosing the cut-off frequency of the low pass filter and the angular and linear sampling intervals causes the appearance of such artifacts.

For example: Aliasing occurs when too few angular views are used, most noticeable toward the periphery of the image. Filling the sampling requirement is needed to avoid such condition (Cherry, 2003). Ring artifacts are also another set of artifacts that can appear during the reconstruction. They are usually caused by applying a low-pass filter to the FT data. Filters with different parameters can be used to avoid this artifacts (Bracewell, 2000).

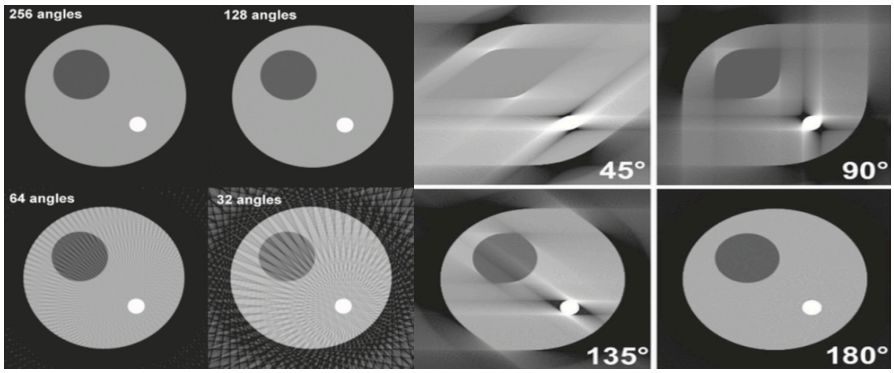

(a) **(b)**

Figure 3.8: Artifacts due to image reconstruction. (a) Number of angular samples effect (b) Angular sampling range effect (Cherry, 2003)

3.9 Nuclear Medicine Imaging (PET)

3.9.1 PET brief history

In the early 1950s, the incorporation of positron emitting isotopes into molecular imaging was recommended for better detection efficiency. This is due to the fact that they could perform better than the traditional techniques employing isotopes that emit a single photon e.g SPECT.

In 1950, Gordon L. Brownell gave the direction to design the first prototype of PET scanner employing two opposite NaI detectors coupled to a PMT. This system uses coincidence detection mechanism and was built within six months in the physics laboratory of Massachusetts General Hospital. Afterwards, brain tumor screening was done with the device, and in 1951 the results were published. In that particular year, an independent exam on annihilation radiation detection was performed and published by Good, Handler and Wrenn. In 1953, an attempt into 3-D data recording was done.

Figure 3.9: First clinical PET **(“**First clinical positron imaging device”, 2017)

In 1952, the first clinical PET device was built (Figure 3.9). It was based on the same concept with that produced in 1950 but it included some transformations. Low resolution images were obtained with such device but it had the sensitivity to suggest the existence of a tumor.

In the middle 1960s, another commercial prototype was developed and the results were published in 1968. This system was a brain dedicated scanner used in the hospital for almost 10years.

The first tomographic imaging PET device known as PC-1 (Figure 3.10) was designed in 1968 and finished in 1969. Tested in 1971 and reports were available in 1972.

David Chesler (1970) designed and tested the FBP through computer simulation. This algorithm was used on the data from PC-1.

In 1971-1976, an improved version of PC-1 the so-called PC-11 was constructed. It employs a rotate-translate mechanism.

In 1973 and 1975, a proposal of systems with ring mechanism was published. They employ several detectors coupled to small PMTs so that good quality images will be reconstructed by means of increasing the number of sampling.

Nowadays, there are several research areas which focus on improving PET systems to achieve high sensitivity and spatial resolution. These areas include scanner geometries, detector materials, image reconstruction techniques and radiopharmaceuticals.

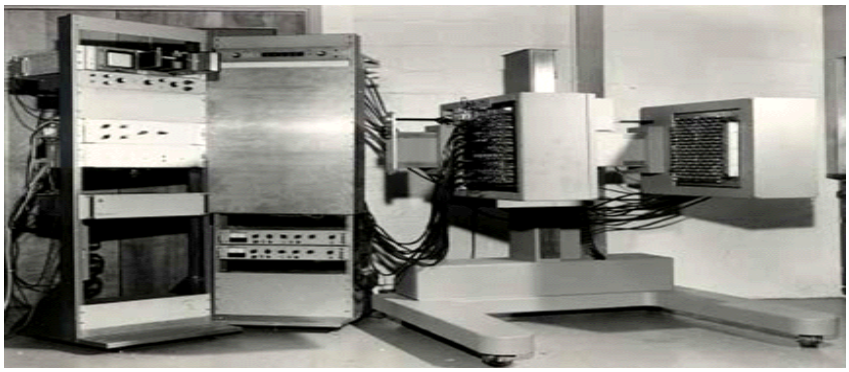

Figure 3.10: First tomographic imaging PET device PC-1 **(“**First clinical positron imaging device”, 2017)

3.9.2 State of the art PET scanners

Modern day systems use scintillator detectors due to their low cost and good stopping power. The crystals are arranged in block manner and they are pixelated via mechanical pixelation into smaller elements coupled to PMT (Figure 3.11). An opaque reflective material is used to fill the channels between the elements, this restrict the optical spill over between elements and enhance sharing of light among the PMTs.

Spatial resolution of the scanners is determined by the width of the detector elements and is 3 to 5 mm in modern PET scanners. Very good SNR is achieved through the use of PMTs for low light levels. On the other hand, their disadvantage is low efficiency in emission. Another disadvantage is that as a scintillator photon deposit its energy, a photo-electron escapes from the cathode part of the PMT.

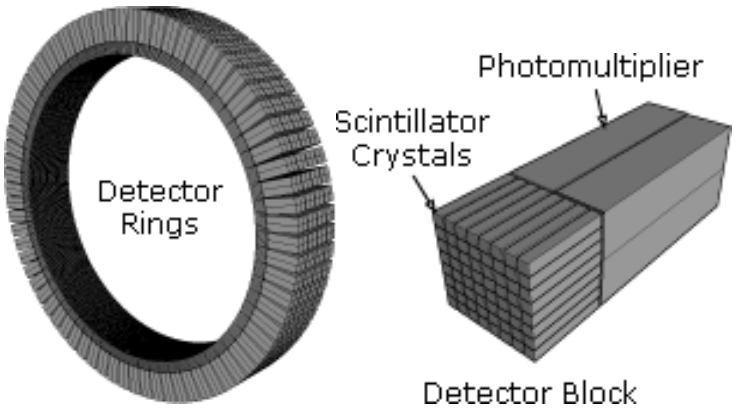

Figure 3.11: Typical geometry of modern PET systems (Valk et al., 2011)

An improvement was made to the PMT used in the scanner, a system known as quadrant sharing where by it covers four quadrants of four detector elements. This is done in order to minimize the number of PMTs used in the scanner. The spatial resolution of such designs is improved, because it allows smaller crystals to be used. Yet, it has a drawback related to dead time because signals from large number of PMT needs to be analyzed.

Good spatial resolution together with short dead time can be achieved by using one-to-one coupling, that is, a single crystal attached to an individual photo-detector. Secondly, small crystals can be coupled to each channel of a Multi-Channel PMT (MC-PMT) or Position Sensitive PMT (PS-PMT).

Instead of PMTs, Avalanche Photo Diodes (APDs) could be an option. The APDs improve SNR by providing an internal amplification of the signal. They can also be employed in hybrid PET/MRI systems because they are not affected by strong magnetic field.

Furthermore, Silicon photomultipliers (SiPMs) can also be used. The SiPMs have ability for input signal amplification (high gain), fast response and low bias voltage. Therefore, they are also good substitute to traditional PMTs.

3.10 PET Clinical Applications

PET plus FDG are used for cancer diagnosis which include the lung, breast, brain etc. They are also used to diagnose brain diseases like Alzheimer's disease, Parkinson's disease and epilepsy. Furthermore, PET has record a great success in the diagnosis of cardiovascular diseases and also to determine the extent of damage done to the heart muscles. They can also be used to measure blood circulation.

3.11 PET in Research

Some PET systems design and development are not meant to be used in clinical applications, rather for research purpose. They are the pre-clinical or small-animal PETs characterized by a small FOV, better image quality, high sensitivity, and lower cost. They have certain advantages such as study of disease model and evaluation of radiotracers in animal models.

Studies involving animal models permits the development of new radiotracers and assessment of new pharmaceuticals. In order to model human disease and understand

mammalian biology, the mouse is a suitable agent. The physiology and genes of mice are similar to that of humans. Furthermore, the rapid reproduction rate of mouse makes the studies more economical, plus mouse colonies maintenance is cheap. Rat models are important in neuroscience because the large rat brain gives ease in surgical procedures, and also during anatomical and developmental studies. Features of Pre-clinical PET systems include narrow timing window, random coincidences minimization, small FOV, high sensitivity and spatial resolution, limited random and scattered coincidences.

3.12 Future PET Generations

Nowadays, developmental trend in PET include: Time-of-fight (TOF) PET, Hybrid imaging (PET/MRI, PET/CT, SPECT/CT) and Semiconductor-based PET systems.

3.12.1 TOF PET

With TOF PET, one can easily locate the position of annihilation without necessarily reconstructing multiple line of responses. This is possible because TOF utilizes the arrival times of annihilation photons and assign greater weight on the the photon that arrives first. The difference in arrival times help to identify the point of annihilation between the two detectors.

Annihilation photons need a time in order of hundreds of picoseconds to reach the detector, this timing is far below the timing resolution of available scanners. Scanners that employ fast crystals have the ability to locate the annihilation event along a line section other than the full line. These scanners are referred to as TOF PETs. Improved SNR is an advantage of such systems because annihilation point is estimated rather than gotten from reconstructed images which suffers from noise propagation.

3.12.2 Hybrid imaging

Hybrid imaging is a new technology in the field of nuclear medicine, it involves a combination of a nuclear device and a radiology device using special software. For instance, PET/MRI is a form of hybrid imaging technique that fuses PET and MRI. During a single imaging session, structural and functional information of cells, tissues, as well as information about blood flows in the body could be revealed. Combination of such systems

provide both anatomical and metabolic images of diagnostic importance (Harberts & Helvoort, 2014).

PET/CT is a form of hybridization in nuclear medicine that combines CT and PET scanner. In this system, the functional images obtained from PET can be combined with anatomical image from CT scan. A radioactive substance is injected into the patient's body just as explained earlier. After uptake period, the patient is placed on the PET/CT bed. Scanning starts from the CT component of the machine to acquire x-ray tomogram and then subsequently to the PET component to acquire metabolic images. Advantages of these systems are that a better localization and metabolic activity could be determined. Lastly, the acquired data are fused together to form PET/CT image (Beyer et al., 2000).

SPECT/CT is a form of hybrid imaging technique which allows the fusion of structural and functional information. With the aid of SPECT/CT, tumor or lesion localization is enhanced due to the combination of functional image and anatomical image. The sensitivity as well as the specificity of findings is improved by the addition of anatomic information (Andreas et al., 2008).

3.12.3 Semiconductor-based PET systems

These systems use semiconductor crystals like CZT or CdTe unlike the conventional systems based on scintillator crystals. The use of semiconductor crystals provides excellent energy resolution. Few examples of the systems employing this crystal are the dedicated cardiac SPECT scanners developed by Digirad corporation and Spectrum dynamics Israel, and the small animal SPECT systems developed by Gamma Medica and GE healthcare.

CHAPTER 4
SYSTEM SPECIFICATIONS, SIMULATION, AND PERFORMANCE EVALUATION OF THE SCANNER

4.1 System Specifications

The system specifications incorporated in the MB-PET is done in such a way to overcome certain limitations of inorganic scintillator crystals. The result presented at the end of this work are from GATE simulation, and can be relied upon because several scanners simulated using the software have been tested and validated.

Features of the PET scanner include:

- High quantum detection and conversion efficiency for 511keV photons due to the high density and atomic number of LYSO (7.1 g/cm^3 and 60 respectively)
- High intrinsic spatial resolution due to high crystal pixelation
- DOI measurement due to small voxels in the crystal.
- Short decay time of 41ns to allow fast response

This PET design can be employed on different types of PET scanners, whether a small-animal, a whole-body and even a PEM scanner. The design implemented here is dedicated to human brain because of the pathologies associated with the brain and the challenges faced while examining the human brain. It allows scattered events arising from the human skull (high density material in the FOV) to suppressed, of which their presence leads to noisy images and low contrast.

The MB-PET scanner (Figure 4.1) takes a modular pattern where each module is a block of LYSO crystal with size 3 cm, 4 cm and 24.4 cm on the x, y, and z directions respectively. For accurate photon impact point measurement, each module block is highly segmented into 9760 mm^2 voxels of $1\times1\times10$ mm^3. Lastly, the module is repeated 48 times to obtain a cylindrical PET system with a total of 468,480 voxels.

The whole detector module faces the center of the cylinder with its active part, thereby allowing 511keV photons to enter from the edge of the LYSO crystal. The superb density of LYSO crystal gives it a superior stopping power over other scintillator crystals. The

complete scanner has a 35.0 cm detector ring diameter, axial FOV of 24.5 cm and trans-axial FOV of 31.0 cm. The system specifications are shown in Table 4.1.

Table 4.1: System specifications

Geometry Design	
Detector size (cm^3)	3 x 4 x 24.4
Detector voxel size (mm^3)	1 x 1 x 10
Number of detector modules	48
Detector ring diameter (cm)	35
Trans-axial FOV (cm)	31
Axial FOV (cm)	24.5
Crystal	LYSO

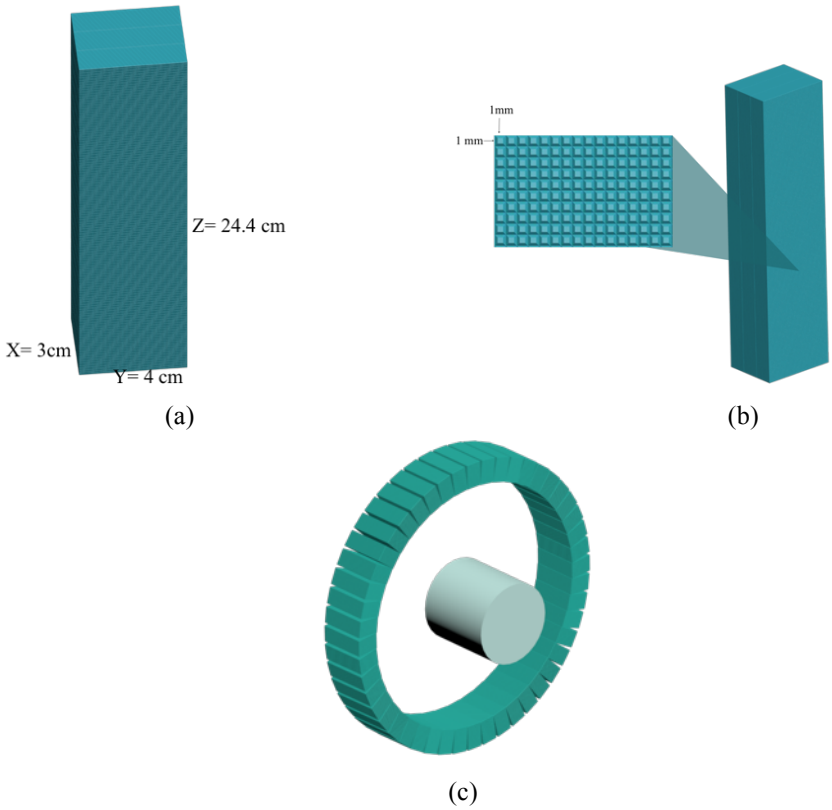

(a) (b)

(c)

Figure 4.1: GATE images of the MB-PET. (a) Detector module (b) detector module with a pixelated section (c) Complete scanner comprising of 48 detector modules.

4.1.1 Advantages and disadvantages

The proposed PET design has several advantages and disadvantages when compared to other PET systems made from scintillator crystals and solid-state crystals. The advantages include:

Ability to obtain an ideal LOR with DOI measurement due to the use of laser technique to segment the crystal block. Back then, this couldn't be achieved because the conventional method is mechanical pixelation which doesn't permit segmentation down to smaller sized pixel leading to a limitation in the system's spatial resolution.

Another advantage is that the system doesn't need many crystal blocks in the module, a single module can be used and pixelated into the desired size and thickness, and achieve high performance at the same time.

Moreover, organ dedicated scanners improve the tumor detectability of a particular organ, plus a reduced field of view that increases the system sensitivity and minimizes scatter. PET scanners employing such specifications are often capable of achieving high performance at low cost.

The disadvantage of such PET system is that, their wide energy window arising from poor energy resolution usually degrades the image quality because weak gamma photons are allowed to be detected by the scanner. This contributes to blurring in the final image.

Another disadvantage is high number of channels, but a technology that handles such numerous channels is available and proposed in (Blanchot et al., 2006).

4.2 Simulations

The MB-PET was simulated using Geant4 Application for Emission Tomography (GATE version 7.2). GATE is a Monte Carlo simulation that plays an important role in new imaging systems design and acquisition protocol optimization. It can also be used to assess or develop correction techniques and reconstruction algorithms. GATE contains the Geant4 library to actualize a versatile, modular and scripted simulation toolkit suitable for use in the nuclear medicine field. It permits an exact simulation of the interaction between a particle and a material within a prescribed scanner geometry, and it has also played an important role in the characterization of time-dependent processes (Jan et al., 2004).

4.2.1 The GATE simulation tool kit

The simulation toolkit contains the Geant4 libraries and it is dedicated specifically to nuclear medicine field. The software can be used over and over in different context because of the similar concept shared by many nuclear medicine diagnostic techniques.

GATE features include an application layer and the user layer, it also has a developer layer that incorporate the application layer and core layer. There are some base classes in the core layer that are common or compulsory in all Geant4-based simulations, they include the ones in geometry construction, physics interaction etc.

The user layer, provides a platform for running simulations batch-wise or interactively using scripts. Therefore, with the use of script language one can easily define a full set-up of a nuclear medicine experiment.

Systems: The concepts used in the systems includes one or more rings that contains the detector module. Modules to scintillator blocks which are segmented into crystal pixels.

Time dependent processes: Time-dependent process management is a unique feature of GATE (Santin *et al.,* 2003). Simulation of realistic acquisition conditions can be achieved because of the synchronization of the geometry with source kinetics. This include patient movement, cardiac and respiratory motions, changes in activity distribution over time or scanner rotation.

Digitizer: Permits the simulation of the electronics response of a detector within a scanner.

Simulation benchmarks: They provide examples of how to use the main features of GATE to simulate PET or SPECT experiments.

Validation of GATE: To assess the accuracy of GATE, one essential method is to validate the simulated data against real data obtained with PET and SPECT cameras. GATE validation has been done and can be found in (Jan et al., 2004).

4.3 Performance Evaluation of the PET Scanner

4.3.1 Sensitivity

Sensitivity is the ability of PET scanners to detect coincident photons from inside the FOV of the scanner. The stopping power of the detectors and the geometry of the scanner largely affects the system sensitivity. The common unit is counts per second per Becquerel (cps/Bq). High-sensitivity scanners are those with large axial FOV and small-diameter

geometry. In general, higher sensitivity leads to good SNR in the reconstructed image. The sensitivity (S_i) at each axial position i, is determined using:

$$S_i = \left(\frac{R_i - R_{B,i}}{A_{cal}}\right) \quad (4.1)$$

where A is the source activity measured in Bq, R_i represent total counts rate (cps) collected in source position (slice) i, and $R_{B,i}$ represent background event rate obtained with no source in the scanner FOV.

For acquisition i, the relative sensitivity is given by:

$$S_{A,i} = \frac{S_i}{0.9060} \times 100 \quad (4.2)$$

where 0.9060 represent the branching ratio of ^{22}Na. To compute the total system sensitivity, the equation below is used. N represent total number of image slices (source positions).

$$S_{tot} = \frac{1}{\mathrm{N}} \sum_{\substack{all \\ i}} S_i \quad (4.3)$$

$$S_{A,tot} = \frac{1}{\mathrm{N}} \sum_{\substack{all \\ i}} S_{A,i} \quad (4.4)$$

The sensitivity test requires that a ^{22}Na point source of less than 0.3 mm diameter with activity of 1MBq be embedded inside an acrylic cube with sides 10 × 10 × 10 mm (Figure 4.2). Six (6) measurements in total were analyzed. The source was positioned at the CFOV of the system to acquire the first measurement. 10^6 coincidences were obtained at the CFOV. Average of all sensitivities is calculated for each source position using equation 4.1, $R_{B,i}$= 0 in the case of simulation.

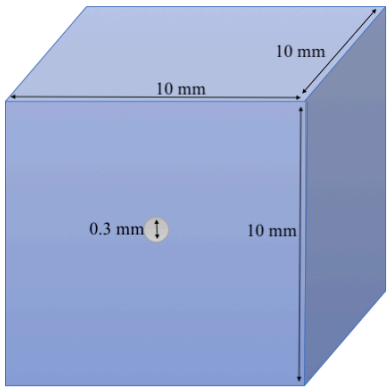

Figure 4.2: Sensitivity measurement phantom

4.3.2 Scatter fraction

This test is done to determine the sensitivity of the system to scattered radiation. The measurement of such events is done at a low counting rate in order to neglect the pileup, random coincidences, and dead-time effects. Scatter fraction for each slice is given in equation 4.5 whereas the mean SF is given in equation 4.6.

$$SF_i = \frac{\frac{C_{s,i,1}}{A_{ave,1}} + 8\left(\frac{C_{s,i,2}}{A_{ave,2}}\right) + 10.75\left(\frac{C_{s,i,3}}{A_{ave,3}}\right)}{\frac{C_{TOT,i,1}}{A_{ave,1}} + 8\left(\frac{C_{TOT,i,2}}{A_{ave,2}}\right) + 10.75\left(\frac{C_{TOT,i,3}}{A_{ave,3}}\right)} \quad (4.5)$$

$$SF = \frac{C_S}{C_{TOT}} \quad (4.6)$$

where C_s represent scattered counts for slice *i,* $C_{TOT,i}$ represent the scattered plus the true counts, and A_{ave} represent the mean radioactivity during acquisition. The numbers *1*, *2*, and *3* represent the radial locations within the phantom.

No matter the effectiveness of a scatter correction process, a low scatter fraction is preferable. The reason behind this is that, those employed correction techniques cannot fix the noise introduced by undesired events.

In order to test for the scatter fraction (SF) of the MB-PET, NEMA NU 4-2008 suggest that a cylindrical phantom (Figure 4.3) made of polyethylene, with 70$\pm$ 0.5 mm length and 25$\pm$0.5 mm diameter be used. The cylinder has a 3.2 mm diameter opening at radial distance of 10 mm and it is parallel to d central axis. A line source 60 mm long with an outside diameter that can fit the 3.2 mm opening of the phantom, is made of flexible tubing with a fillable section 10 mm less than the phantom. It contains a known quantity of radioactivity and is inserted into the 3.2 mm hole. Low source activity should be used so that the random events rate can be below a percent of the true event rate. The test recommends placing the phantom in the CFOV parallel to the z-axis. For the SF calculation, minimum of 500,000 coincidences should be obtained. The source used was ^{18}F, and the activity was 10 MBq.

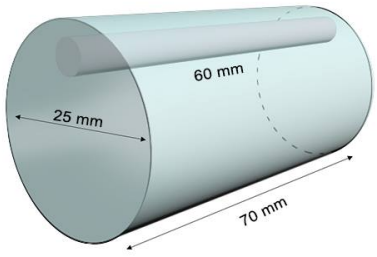

Figure 4.3: Scatter fraction phantom

4.3.3 Spatial resolution

The ability to distinguish between two points of radioactivity in an image is known as spatial resolution. This measurement is done on the reconstructed image of compact radioactive sources in order characterize the widths of the point spread function (PSF). Full width at half maximum (FWHM) and full width at tenth maximum (FWTM) are the terms used to describe the spatial resolution of a given system. Measurements are done in the radial and tangential direction of the transverse slice, and also on the axial direction.

The same phantom for sensitivity test was used. Per measurement, minimum of 10^5 coincidences were collected and MLEM algorithm was used to reconstruct the images.

4.3.4 NEMA image quality

The test is performed using a phantom made of polymethylmethacrylate (Figure 4.4). It has five fillable rods of 1 mm, 2 mm, 3 mm, 4 mm, and 5 mm respectively. The chamber of the main body and the rods are filled with ^{18}F radioactive water of 3.7 MBq total activity. It has two chambers at the top section, one is filled with air and the other with water (non-radioactive) so that two cold regions can be formed.

Images were reconstructed from 10 million coincidences as required by NEMA NU 4-2008. MLEM was used to reconstruct the images with no corrections applied. Furthermore, normalization is not required because the data are from simulation. The pixel size and slice thickness are 0.25 mm and 2 mm respectively.

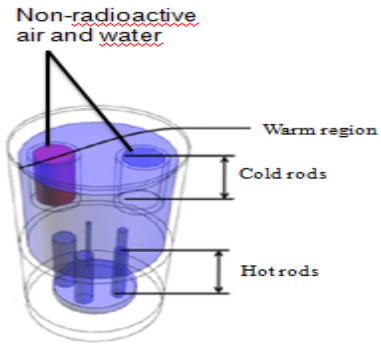

Figure 4.4: NEMA image quality phantom

4.3.5 Uniformity test

The uniformity test is performed using a cylindrical volume of interest (Figure 4.5), it has a length of 10 mm and a diameter of 22.5 mm. The cylinder was traced on the uniform region of the image quality phantom.

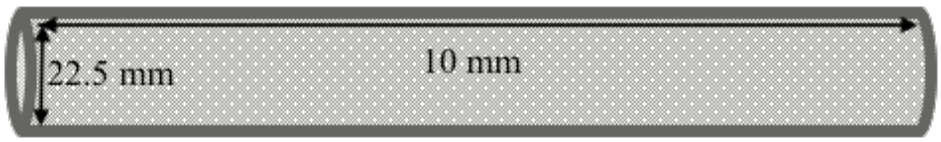

Figure 4.5: Uniformity cylinder

4.3.6 Derenzo-like phantom study

This phantom is a circular piece of plastic that has several rods drilled through. It has 5 sections, each comprises of rods having different diameters and 12 mm length. The rods are filled with 1 MBq of ^{18}F radioactive isotope. The rods used for this particular test are from 1.2 to 3 mm in diameter (Figure 4.6). The phantom images were reconstructed using MLEM, 10 million coincidences were collected and 0.5 x 0.5 x 1.0 mm^3voxel was used.

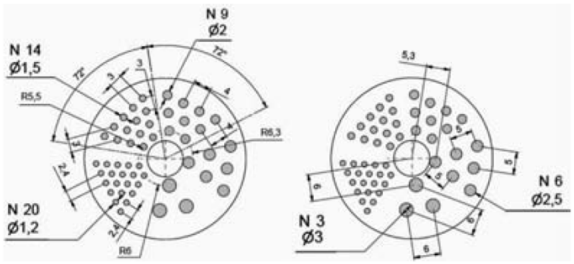

Figure 4.6: Derenzo phantom

CHAPTER 5
RESULTS

5.1: Sensitivity

To measure the system sensitivity, we followed the NEMA NU 4-2008 protocol described in (4.3.1). System sensitivity of 4.8% was achieved by analyzing 6 measurements as shown in Figure 5.1.

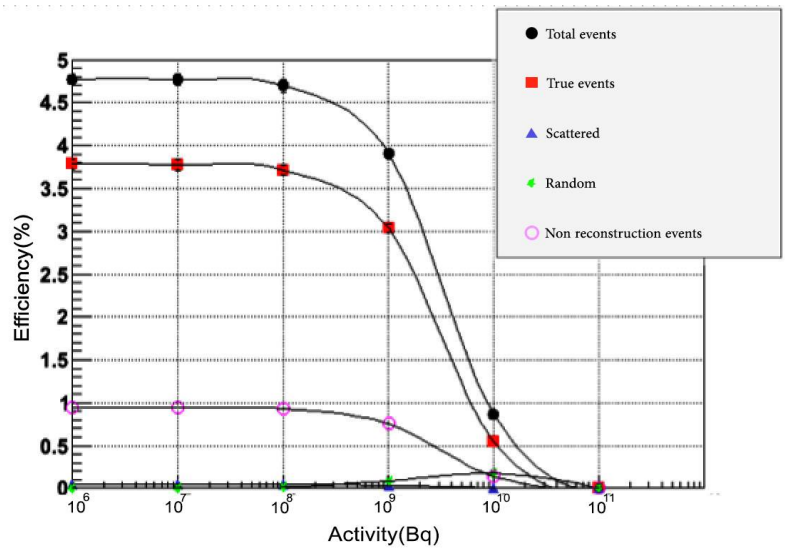

Figure 5.1: System sensitivity of the PET scanner, no correction technique applied

Table 5.1: Comparison of sensitivity between the MB-PET and other PET systems

Brain PET scanners	Sensitivity (%)	Energy window (keV)
MB-PET	4.8	350-650
ECAT HRRT	4.3	250-650
HRRT-D	3.3	350-650
HOT-PET	9.2	300-675
JPET-D4	11	400-600

Based on the values shown in Table 5.1, the sensitivity of MB-PET can be averagely classified. Although some of the scanners have higher sensitivity values, due to wider energy window (HOT-PET), and the use of multiple rings of detector (JPET-D4).

5.2 Scatter Fraction

Scatter fraction measurement follows the description in (4.3.2). In simulations, the exact number of random event, true event, scattered event, and the source radioactivity (1MBq) are known. Therefore, the calculated mean SF of the system is 48%.

Table 5.2: Comparison of SF between the MB-PET, G-PET and HRRT ECAT

Brain PET scanners	Scatter Fraction (%)	Energy window (keV)
MB-PET	48	350-650
G-PET	39	410-665
HRRT ECAT PET	52.9	250-650

From Table 5.1, it can be seen that the MB-PET has a scatter fraction result close to that of other scanners employing scintillator crystals. It is worthy to note that scintillator based PET scanners are normally characterized with high scatter fraction value. The SF was compared to above-mentioned scanners, because their performance was tested using the same procedure.

5.3 Spatial Resolution

NEMA NU 4-2008 standard was used as described in (4.3.3). FWHM values for the measured PSF in all three directions were determined and are shown in Table 5.1. Spatial resolution results are approximately 1.03 to 2.05 mm in the axial direction and 1.01 to 1.28 mm in the trans-axial direction.

Table 5.3: Spatial resolution results

Positions (mm)	0	10	100
Radial resolution	1.01	1.02	1.28
Tangential resolution	1.01	1.21	1.41
Axial resolution	1.03	1.27	2.05

Table 5.4: Comparison of spatial resolution result with other brain PET scanners

Brain PET scanners	Spatial resolution (mmFWHM)
MB-PET	Axial = 1.03 to 2.05 trans-axial = 1.01 to 1.28
ECAT HRRT	Axial = < 2.4
HRRT-D	Axial = 2.5 to 3.4 trans-axial = 2.3 to 3.2
HOT-PET	Axial = 2.8 to 3.9 trans-axial = 2.7 to 4.0
JPET-D4	Axial = < 3

From the above table, it is obvious that MB-PET has an improved spatial resolution compared to other brain PET scanners, this is due to the high intrinsic spatial resolution of the crystal used.

5.4 Image Quality Test

The test is performed as described in (4.3.4). The phantom was placed at the system's CFOV. Figure 5.2 shows the emitting point digital map image and the reconstructed image, whereas Figure 5.3 shows the corresponding line profiles.

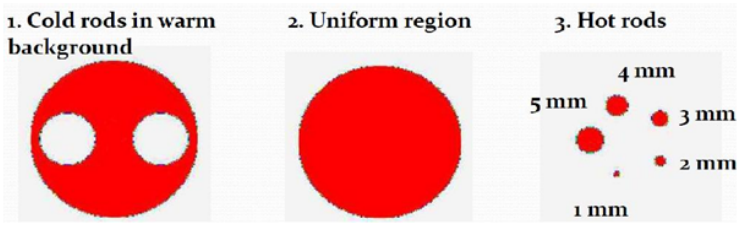

(a)

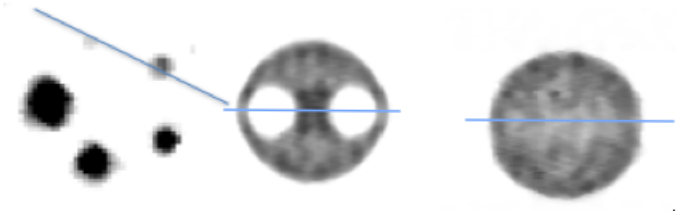

(b)

Figure 5.2: NEMA image quality phantom images: (a) emitting point digital map image, (b) reconstructed images: Left to right: hot rods, cold inserts, and uniform region

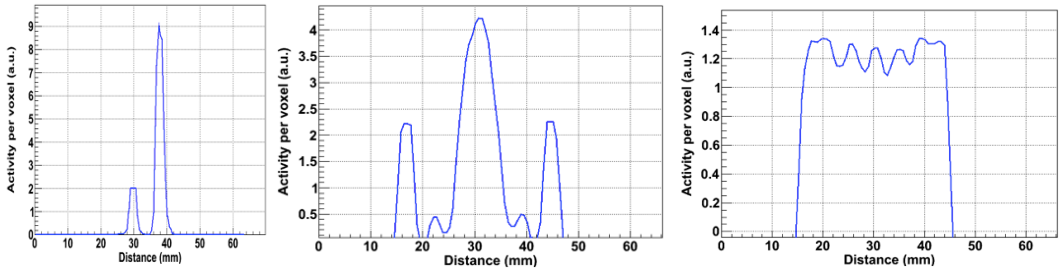

Figure 5.3: Line profiles of the reconstructed phantom images

5.5 Uniformity Test

The uniformity test is performed using the cylinder described in (4.3.5). The reconstructed image and the corresponding line profile is shown in Figure 5.4.

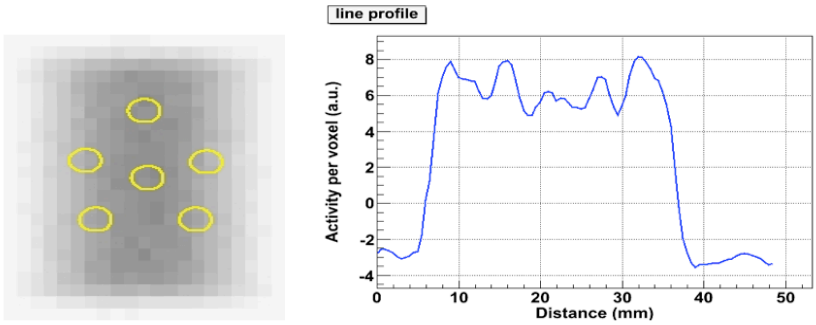

Figure 5.4: Reconstructed Image of uniformity test and corresponding line profile

5.6 Derenzo-like Phantom Study

The performance of the scanner was also evaluated using Derenzo phantom described in (4.3.6). Figure 5.5 shows the emitting point digital map image, reconstructed image, and corresponding line profile, it also shows that 1.2 mm hot spheres are resolvable with no correction technique applied.

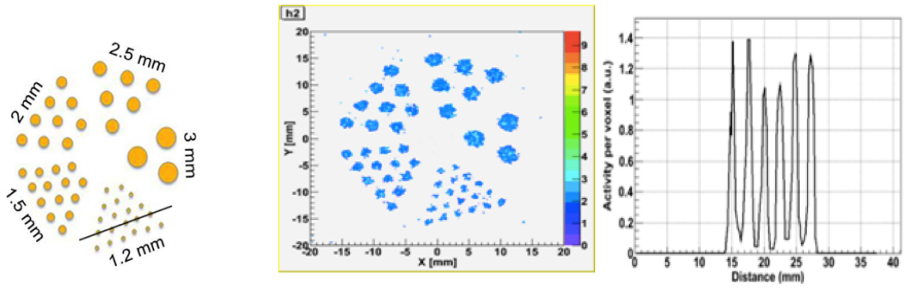

(a) (b)

Figure 5.5: Derenzo phantom images (a) emitting point digital map image, (b) reconstructed image and corresponding line profile

CHAPTER 6
CONCLUSIONS AND RECOMMENDATIONS

6.1 Conclusions

The results presented in this thesis are based on GATE simulation. The parameters used to simulate the scanner geometry are from a particular technical design. The concept used to simulate the detector is from a published work on fabricating scintillator crystals using LIOB technique. The image quality, sensitivity, spatial resolution, scatter fraction, uniformity and Derenzo phantom performance evaluation of the simulated scanner were performed with NEMA protocol. The small scanner's geometry combined with the stopping power of 3 cm for LYSO crystal gave the MB-PET a sensitivity of 4.8%. The sensitivity is quite encouraging when compared to other scintillator based PET scanners. The high scatter fraction obtained is really discouraging, though its due to the poor energy resolution of scintillator crystals. From previous published works, it was shown that scintillator crystals are characterized with such high scatter fraction. Images were reconstructed using MLEM algorithm with no correction applied. This algorithm gives precise results, but happens to be slow when compared to other algorithms like FBP.

Excellent spatial resolution (1 mm) in the CFOV was achieved according to NEMA NU4 - 2008. This study shows that the PET scanner is capable of achieving higher spatial resolution and sensitivity at low cost. From previous published studies, it was evident that pre-clinical systems were the ones with such capability. The result also showed that the system is capable of resolving 1.2 mm hot rods with no correction technique applied. This study provides results that shows the potentials of scintillator-based PET scanners at achieving good performance at lower-cost.

Lastly, Simulation results reveal that the MB-PET, if developed will solve the problems of missing brain tumors, and enhance tumor diagnosis.

6.2 Recommendations

For future related study, other crystals and different system design can be adopted to improve the system sensitivity and spatial resolution of Brain PET scanners. In addition, related studies should be conducted in other to aid accurate diagnosis of brain tumors for better patient health and chances of survival from brain related diseases.

REFERENCES

Aarsvold, J., and Wernick, M.N. (2004). Emission Tomography: The Fundamentals of PET and SPECT. Burlington: Elsevier.

Alessio, A., and Kinahan, P. (2006). PET Image Reconstruction. New York, NY: Elsevier.

Andreas, K.B., Stephan, N., Sibylle, Z., Ambros, B., Bernd, J.K., Ken, H., … Alexander, D. (2008). SPECT/CT. *Journal of Nuclear Medicine, 49*(8), 1305-1319.

Asl, M., and Sadremomtaz, A. (2013). Analytical image reconstruction methods in emission tomography. *Journal of Biomedical Science and Engineering*, *06*(01), 100-107. http://dx.doi.org/10.4236/jbise.2013.61013

Badawi, R.D., and Marsden, P.K. (1999). Developments in component-based normalization for 3D PET. *Physics in Medicine and Biology, 44*(2), 571-594. http://www.ncbi.nlm.nih.gov/pubmed/10070802

Bailey, D., Maisey, M., Townsend, D., and Valk, P. (2005). Positron Emission Tomography. London: Springer-Verlag.

Beyer, T., Townsend, D.W., Brun, T., Kinahan, P.E., Beyer, T. (2000). A combined PET/CT scanner for clinical oncology. *The Journal of nuclear medicine, 41*(8), 1369-1379.

Brain Tumor: Statistics. (2017, November 13). Retrieved from https://www.cancer.net/cancer-types/brain-tumor/statistics

Braem, A., Chamizo Llatas, M., Chesi, E., Correia, J.G., Garibaldi, F., Joram, C., … Zaidi, H. (2004). Feasibility of a novel design of high resolution parallax-free compton enhanced PET scanner dedicated to brain research. *Physics in Medicine and Biology, 49*(12), 2547-2562.

Cherry, S.R., and Huang, S-C. (1995). Effects of scatter on model parameter estimates in 3D PET studies of the human brain. *IEEE Transactions on Nuclear Science, 42* (4), 1174-1179.

Cherry, S.R., Sorenson, J., and Phelps, M. (2012). Physics in Nuclear Medicine. Philadelphia, Pa: Saunders.

Cherry, S.R., and Dahlbom, M. (2004). PET: Physics, Instrumentation and Scanners (pp. 1-124). New York, NY: Springer. http://dx.doi.org/10.1007/978-0-387-22529-6_1

Cradduck, T.D., and Busemann-Sokole, E. (1985). Computers in nuclear medicine. *RadioGraphics, 5*(1), 52-60.

Curry, T., Dowdey, J., Murry, R., and Christensen, E. (1990). Christensen's Physics of Diagnostic Radiology. Philadelphia: Lea & Fibiger.

Discovering the positron. (2017, August 21). Retrieved from http://timeline.web.cern.ch

Du, J., Wang, Y., Zhang, L., Zhou, Z., Xu, Z., and Wang, X. (2009). Physical properties of LYSO scintillator for NN-PET detectors. *In Proceedings of the 2nd International Conference on Biomedical Engineering and Informatics (pp. 1-5)*. Tianjin, China. http://dx.doi.org/10.1109/bmei.2009.5305107

First Clinical Positron Imaging Device. (2017, August 11). Retrieved from http://www.petdiagnostik.ch/de/informationen-fuer-fachpersonen/a-history-of-positron-imaging/first-clinical-positron-imaging-device---1952.php

Flickr (2006). Pair production. Retrieved August 26, 2017 from https://www.flickr.com/photos/mitopencourseware/4706123553

Harberts, D.W., and Van Helvoort, M. (2014). Sensitivity of a 1.5-T MRI system for electromagnetic fields. *In Proceedings of the International Symposium on Electromagnetic Compatibility (pp. 856-859)*. Gothenburg, Sweden.

Imagingkt (2016). Physical Interaction processes. Retrieved August 26, 2017 from http://199.116.233.101/index.php/Physical_Interaction_processes

Jan, S., Santin, G., Strul, D., Staelens, S., Assié, K., Autret, D., … Morel, C. (2004). GATE: A simulation toolkit for PET and SPECT. *Physics in Medicine and Biology, 49*, 4543-4561.

Jemal, A., Siegel, R., Xu, J., and Ward, E. (2010). Cancer statistics. *CA Cancer Journal for Clinicians, 60*(5), 277-300. doi:10.3322/caac.20073

Jong, H., Velden, F., Kloet, R., Buijs, F., Boellaard, R., and Lammertsma, A. (2007). Performance evaluation of the ECAT HRRT: an LSO-LYSO double layer high resolution, high sensitivity scanner. *Physics in Medicine and Biology, 52*(5), 1505-1526.

Kamal, A. (2014). Nuclear Radiation Detectors. In: Particle Physics. Berlin: Springer http://dx.doi.org/10.1007/978-3-642-38661-9_1

Karp, J.S., Surti, S., Daube-Witherspoon, M.E., Freifelder, R., Cardi, C.A., Adam, L., …

Muehllehner, G. (2003). Performance of a brain PET camera based on anger-logic gadolinium oxyorthosilicate detectors. *The journal of nuclear medicine, 44*(8), 1340-1349.

Kinahan, P., Defrise, M., and Clackdoyle, R. (2004). Analytic image reconstruction methods. *Emission Tomography*, 421-442. http://dx.doi.org/10.1016/b978-012744482-6.50023-5

Knoll, G. (2010). Radiation detection and measurement. Hoboken, N.J: John Wiley.

Kolstein, M., Mikhaylova, E., De Lorenzo, G., Chmeissani, M., Arino, G., Calderon, Y., and Ozsahin, D.U. (2013). Evaluation of origin ensemble algorithm for image reconstruction for pixelated solid-state detectors with large number of channels. *Journal of Instrumentation, 8*, P04030.

Krane, K.S. (1987). Introductory Nuclear Physics. New York, NY: John Wiley & Sons.

Levin, C.S., and Hoffman, E.J. (1999) Calculation of positron range and its effect on the fundamental limit of positron emission tomography system spatial resolution. *Physics in Medicine and Biology, 44*(3), 781-799.

Lodge, M.A., Badawi, R.D., Gilbert, R., Dibos, P.E., and Line, B.R. (2006). Comparison of 2-dimensional and 3-dimensional acquisition for ^{18}F-FDG PET oncology studies performed on an LSO-based scanner. *Journal of Nuclear Medicine, 47*, 23-31.

Maligs, F. (2017). Filtered back projection. *Radiology Reference Article*. Retrieved September 27, 2017 from https://radiopaedia.org/articles/filtered-back-projection-1

Martins, M. (2015). Mammography Techniques and Reviews. Croatia: INTECH http://dx.doi.org/10.5772/60452

Mikhaylova, E. (2014). Voxel Imaging PET Pathfinder: A novel approach to positron emission tomography based on room temperature pixelated CdTe detector. *Doctoral thesis*, *Universitat Autonoma de Barcelona*, Barcelona, Spain.

Mikhaylova, E., De Lorenzo, G., Chmeissani, M., Kolstein, M., Cañadas, M., Arce, P., … Cabruja, E. (2014). Simulation of the expected performance of a seamless scanner for brain PET based on highly pixelated CdTe detector. *IEEE Transactions on Medical Imaging, 33*(2), 332–339. doi:10.1109/TMI.2013.2284657

Morimoto, Y., Ueno, Y., Takeuchi, W., Kojima, S., Matsuzaki, K., Ishitsu, T., … Tamaki, N. (2011). Development of a 3D brain PET scanner using CdTe semiconductor

detectors and its first clinical application. *IEEE Transactions on Nuclear Science, 58*(5), 2181-2189.

NEMA Standards Publication (2008). Performance Measurements of Small Animal Positron Emission Tomographs. Rosslyn, VA: National Electrical Manufacturers Association.

Nikl, M. (2006). Scintillation detectors for X-rays. *Measurement Science and Technology*, *17*(4), R37-R54. http://dx.doi.org/10.1088/0957-0233/17/4/r01

Patching, S. (2015). Roles of facilitative glucose transporter GLUT1 in [^{18}F] FDG Positron Emission Tomography (PET) imaging of human diseases. *Journal of Diagnostic Imaging in Therapy, 2*(1), 30-102. doi: http://dx.doi.org/10.17229/jdit.2015-0301-014

P-N Junction Theory for Semiconductor Diodes. (2017, August 28). Retrieved from http://www.electronics-tutorials.ws/diode/diode_2.html

Positron Emission Tomography. (2017). *Radiology Key*. Retrieved October 9, 2017 from https://radiologykey.com/positron-emission-tomography/

Powsner, R., Palmer, M., and Powsner, E. (2013). Essentials of Nuclear Medicine Physics and Instrumentation. Chichester: Wiley-Blackwell.

Radiology key (2016). Interaction of High-Energy Radiation with Matter. Retrieved August 26, 2017 from https://radiologykey.com/interaction-of-high-energy-radiation-with-matter/

Sabet, H., Kudrolli, H., Singh, B., and Nagarkar, V.V. (2012). Fabricating high resolution and high-sensitivity scintillator arrays using laser induced optical barriers. *In Proceedings of the IEEE Nuclear Science Symposium and Medical Imaging Conference* (pp. 4080-4084). Anaheim, U.S.A. doi:10.1109/NSSMIC.2012.6551932

Sabet, H., Bläckberg, L., Uzun-ozsahin, D., and El-Fakhri, G. (2016). Novel laser-processed CsI:TI detector for SPECT. *Medical Physics, 43*(5), 2630-2638. http://dx.doi.org/10.1118/1.4947294

Sabet, H., Blackberg, L., Ozsahin, D., Sitek, A., and El-Fakhri, G. (2015). A sub-mm spatial resolution LYSO:Ce detector for small animal PET. *In Proceedings of the IEEE Nuclear Science Symposium and Medical Imaging Conference (pp. 1-4)*. San Diego, U.S.A. http://dx.doi.org/10.1109/nssmic.2015.7582201

Scintillation counter. (2017, August 28). Retrieved from https://en.wikipedia.org/wiki/Scintillation_counter

Shukla, A.K., and Utham, K. (2006). Positron emission tomography: An overview. *Journal of Medical Physics, 31*(1), 13–21. doi:10.4103/0971-6203.25665

Sossi, V., Pointon, B., Cohen, P., Johnson, R.R., and Ruth, T.J. (2000). Effect of shielding the radioactivity outside the field of view on image quality in a dual head coincidence [PET camera]. *IEEE Transactions on Nuclear Science, 47*(4), 1561-1566. http://ieeexplore.ieee.org/stamp/stamp.jsp?tp=

Staelens, S., Strul, D., Santin, G., Koole, M., Vandenberghe, S., D'Asseler, Y., … Van de Walle, R. (2003). Monte Carlo simulations of a scintillation camera using GATE: validation and application modelling. *Physics in Medicine and Biology, 48*, 3021-42.

Sweet, W.H. (1951). The use of nuclear disintegration in the diagnosis and treatment of brain tumor. *New England Journal of Medicine*, *245*, 875-878.

Takahashi, T., and Watanabe, S. (2000). Recent progress in CdTe and CdZnTe detectors. *IEEE Transaction on Nuclear Sciences, XX*(Y), 101.

Tong, S., Alessio, A., and Kinahan, P. (2010). Image reconstruction for PET/CT scanners: past achievements and future challenges. *Imaging in Medicine*, *2*(5), 529-545. http://dx.doi.org/10.2217/iim.10.49

Uzun, D., De Lorenzo, G., Kolstein, M., & Chmeissani, M. (2014). Simulation and evaluation of a high resolution VIP PEM system with a dedicated LM OSEM algorithm. *Journal of Instrumentation*, *9*(5), C05011. doi:10.1088/1748-0221/9/05/C05011

Valk, P.E., Delbeke, D., Bailey, D.L., Townsend, D.W., and Maisey, M.N. (2011). Positron emission tomography. Clinical practice. Lexington, KY: Springer.

Vandenberghe, S., Mikhaylova, E., D'Hoe, E., Mollet, P., and Karp, J.S. (2016). Recent developments in time-of-flight PET. *European Journal of Nuclear Medicine and Molecular Imaging Physics, 3*(3), 1. doi: 10.1186/s40658-016-0138-3

Van Roosbroeck, W., and Shockley, W. (1954). Photon-radiative recombination of electrons and holes in Germanium. *Physical Review, 94*(6), 1558-1560. doi:10.1103/PhysRev.94.1558.

Watanabe, M., Shimizu, K., Omura, T., Takahashi, M., Kosugi, T., Yoshikawa, E., … Yamashita, T. (2002). A new high-resolution PET scanner dedicated to brain research. *IEEE Transaction on Nuclear Science*, *49*, 634–639.

Wienhard, K., Schmand, M., Casey, M.E., Baker, K., Bao, J., Eriksson, L., … Nutt, R. (2002). The ECAT HRRT: Performance and first clinical application of the new high resolution research tomograph. *IEEE Transactions on Nuclear Science, 49*(1), 104-110.

Wikiwand. (2017, August 26). Proportional counter. Retrieved from http://www.wikiwand.com/en/Proportional_counter

Wong, W-H., Uribe, J., Li, H., Baghaei, H., Wang, Y., Aykac, M., Liu, Y., … Farrell, R. (2002). The design of a high-resolution transformable whole-body PET camera. *IEEE Transactions on Nuclear Science, 49*(5), 2079-2084.

Yamaya, T., Yoshida, E., Obi, T., Ito, H., Yoshikaawa, K., and Murayama, H. (2008). First human brain imaging by the jPET-D4 prototype with a pre-computed system matrix. *IEEE Transactions on Nuclear Science, 55*(5), 2482-2492.

Zaidi, H. (2000). Monte-carlo simulation studies of scatter correction in positron emission tomography. *Doctoral thesis*, *Université de Genève*, Genève, Switzerland. Retrieved from http://www.unige.ch/cyberdocuments/theses2000/ZaidiH/these.html

Zaidi, H., and Hasegawa, B.H. (2003). Determination of the attenuation map in emission tomography. *Journal of Nuclear Medicine, 44*(2), 291-315. http://jnm.snmjournals.org/content/44/2/291